OPEN

Citation: Bone Research (2014) 2, 14034; doi:10.1038/boneres.2014.34

www.nature.com/boneres

ARTICLE

High-throughput screening of mouse gene knockouts identifies established and novel skeletal phenotypes

Robert Brommage, Jeff Liu, Gwenn M Hansen, Laura L Kirkpatrick, David G Potter, Arthur T Sands, Brian Zambrowicz, David R Powell and Peter Vogel

Screening gene function *in vivo* is a powerful approach to discover novel drug targets. We present high-throughput screening (HTS) data for 3 762 distinct global gene knockout (KO) mouse lines with viable adult homozygous mice generated using either gene-trap or homologous recombination technologies. Bone mass was determined from DEXA scans of male and female mice at 14 weeks of age and by microCT analyses of bones from male mice at 16 weeks of age. Wild-type (WT) cagemates/littermates were examined for each gene KO. Lethality was observed in an additional 850 KO lines. Since primary HTS are susceptible to false positive findings, additional cohorts of mice from KO lines with intriguing HTS bone data were examined. Aging, ovariectomy, histomorphometry and bone strength studies were performed and possible non-skeletal phenotypes were explored. Together, these screens identified multiple genes affecting bone mass: 23 previously reported genes (*Calcr*, *Cebpb*, *Crtap*, *Dcstamp*, *Dkk1*, *Duoxa2*, *Enpp1*, *Fgf23*, *Kiss1/Kiss1r*, *Kl* (*Klotho*), *Lrp5*, *Mstn*, *Neo1*, *Npr2*, *Ostm1*, *Postn*, *Sfrp4*, *Slc30a5*, *Slc39a13*, *Sost*, *Sumf1*, *Src*, *Wnt10b*), five novel genes extensively characterized (*Cldn18*, *Fam20c*, *Lrrk1*, *Sgpl1*, *Wnt16*), five novel genes with preliminary characterization (*Agpat2*, *Rassf5*, *Slc10a7*, *Slc26a7*, *Slc30a10*) and three novel undisclosed genes coding for potential osteoporosis drug targets.

Bone Research (2014) **2,** 14034; doi:10.1038/boneres.2014.34; Published online: 28 October 2014

INTRODUCTION

Following successful sequencing of the human and mouse genomes, a major goal of the genomics community has been to determine the functions of the ~20 000 mammalian protein-coding genes by generating and examining phenotypes of knockout (KO) mice for each gene. Initial efforts towards this goal were pursued by Lexicon Pharmaceuticals (summarized in this report) and Deltagen.[1] More recently, academic centers joined forces to form the International Knockout Mouse Consortium (IKMC) encompassing efforts by the Knockout Mouse Project, European Conditional Mouse Mutagenesis Program, North American Conditional Mouse Mutagenesis Program and the Texas A&M Institute of Genomic Medicine[2–6].

From 2000 through 2008, Lexicon Pharmaceuticals performed high-throughput mouse knockout and comprehensive phenotypic analyses (Genome5000™) for >4 650 genes. KO strategies (described below) involved both gene trapping,[7] using the OmniBank® I embryonic stem (ES) cell library, and homologous recombination technologies. Lexicon generated a second ES cell library (OmniBank® II) for the TIGM gene trap repository[8] and since 2009, over 100 studies have used this resource to examine gene disruptions in mice (http://www.tigm.org/publications/). Phenotyping involved a battery of tests in the areas of behavior, cardiology, immunology, metabolism, oncology and ophthalmology, and included serum chemistry, histopathology and a high fat diet obesity challenge. Mice and ES cells from many KOs generated through this Genome 5000™ program are available through the USA NIH Mutant Mouse Regional Resource Center (https://www.mmrrc.org/catalog/overview_Major_Collection.php), Wellcome Trust (http://www.tigm.org/wellcome-trust/) and Taconic Farms (http://www.taconic.com/KO). The USA NIH Mutant Mouse Regional Resource Center collection includes 472 genes analyzed as part of Genentech's Secreted Protein Discovery Initiative[9] and having published phenotypes.[10] Lexicon published body composition data for gene KOs (through 2005) that resulted in lean and obese phenotypes among the first 2 322 KO lines

Lexicon Pharmaceuticals, The Woodlands, TX, USA
Correspondence: R Brommage (brommage@outlook.com)
Received: 16 July 2014; Revised: 29 July 2014; Accepted: 31 July 2014

evaluated.[11] The present report describes the high-throughput screen employed to detect skeletal phenotypes and provides data on genes this screen identified that influence bone mass and architecture.

The International Mouse Phenotyping Consortium (IMPC, http://mousephenotype.org) was launched in September 2001 to coordinate phenotyping efforts of 15 worldwide groups involved in the IKMC.[12–13] Considerable effort and discussions have focused on optimizing these comprehensive high-throughput screens (HTS) to phenotype the mouse gene KOs.[6,14–23] Our goal is not to review current screening protocols, but to describe the successful HTS strategy employed by Lexicon for identifying skeletal phenotypes.

Lexicon's protocol to identify potential skeletal phenotypes involved three complementary analyses: (i) whole body, femur and spine BMD by DEXA scans of anesthetized mice; (ii) microCT scans of dissected bones to determine bone architecture of the LV5 spine vertebral body and midshaft femur; and (iii) histological examinations of decalcified bones (long bones, sternums and nasal turbinates). Full experimental details are provided below.

The goal of HTS is to identify the few genes that influence phenotypes among the many knockouts examined. The conflict between thoroughly studying individual lines of KO mice and examining many different KO lines involves difficult compromises. The number of mice examined, the number of bones examined from each mouse, the skeletal measurements made and the criteria employed to identify potential skeletal phenotypes all must be simultaneously optimized. Undoubtedly, both false positives (genes falsely identified as having KO phenotypes) and false negatives (genes with true KO phenotypes that are missed) occur.

Without confirmation in additional cohorts of mice, phenotypes identified in HTS can represent false positive findings due to the necessity of examining multiple bone parameters in a small number of mice. Bone HTS results reported by three groups all limited their analyses to primary radiographic and DEXA screens. Deltagen[1] examined 750 gene KOs and found 9 (1%) with skeletal phenotypes. Genentech[10] reported 150 of 476 (32%) KO lines showed bone phenotypes. The Wellcome Trust Sanger Institute reported bone phenotypes in 10 of 100 genes[24] and subsequently 9 body BMD and 33 radiographic phenotypes in 146 KOs (of 250 total) with viable mice.[25]

Although the possibility of missing true phenotypes can never be completely eliminated, this risk of false negatives can be estimated by the ability of the HTS to identify previously established KO gene phenotypes. As described below, Lexicon's skeletal HTS successfully confirmed published results of established genes including *Fgf23*, *Klotho*, *Crtap*, *Ostm1* and *Src* and for these genes no further bone measurements beyond HTS were made. For *Lrp5*,[26] *Sost*,[27] *Wnt10b*,[28] *Dkk1*[29] and *Sfrp4*[30] bone phenotypes observed in the HTS were confirmed and extended in subsequent cohorts of mice. Many well-studied genes known to affect bone, such as *Dmp1*, *Ctsk*, *Rank* and *Rankl*, were not examined.

Lexicon's motivation for undertaking this KO and phenotyping program involved identifying novel therapeutic targets.[31–33] This motivation dictated specifically targeting the roughly 5000 genes in the druggable genome[34–35] and the selection of HTS assays measuring phenotypes providing guidance for treatable diseases. Thus, the genes analyzed were highly enriched in enzymes, receptors and secreted proteins, but transcription factors such as *Runx2, Osterix* and *Msx2*, and genes coding for structural proteins were omitted. Abnormalities in developmental processes, such as craniofacial[36] and digit anatomy, and longitudinal bone growth, result in serious human diseases, but are not easily amenable to treatment with small molecule drugs or neutralizing antibodies. For bone, our primary interest involved genes controlling bone formation by osteoblasts and bone resorption by osteoclasts. Identifying novel genes in these pathways can potentially lead to new osteoporosis therapies. Genes involved with diseases directly resulting from gene mutation such as *osteogenesis imperfecta* and chondrodysplasias were examined but not studied extensively, as they are less likely to yield targets for drug development.

Most importantly, given the goal to discover novel genes not previously known to regulate bone mass, Lexicon identified several novel genes, including *Cldn18*, *Fam20c*, *Lrrk1*, *Sgpl1* and *Wnt16*. KO of *Wnt16* reduces cortical bone mass and multiple human GWAS studies subsequently identified SNPs in the *WNT16* gene region that affect cortical bone mass and strength.[37–38] KO of *Lrrk1*[39] produces severe osteopetrosis from osteoclast dysfunction, whereas KO of *Cldn18* results in reduced bone mass from hyperactive osteoclasts.[40] The FAM20C protein was recently established as the kinase phosphorylating secreted proteins[41] and *Fam20c* KO mice have hypophosphatemic rickets.[42] Among other actions,[43] sphingosine-1-phosphate is a key mediator of osteoclast/osteoblast communication[44] and KO of *Sgpl1*[45] results in compromised immune function and osteopetrosis.

MATERIALS AND METHODS

Mouse production

Gene trapping offers a high-throughput approach for producing large numbers of insertional mutations in the mouse genome, while gene targeting by homologous recombination allows precise manipulation of genetic sequences in the mouse. Lexicon utilized both methods to generate KO mice for the Genome 5000™ project. KO mice were generated by homologous recombination

using both a λ phage KOS shuttle system[46] and PCR-based targeting vector strategies as described.[47] Gene trapped lines were derived from the OmniBank® I library.[48] Details of each mutation are provided in Supplementary Table S1. To achieve effective gene disruption when using gene-trap mutations, intragenic insertions intersecting all known transcript units were selected after identifying the precise location of vector insertion using inverse genomic PCR. Oligonucleotide primers complementary to the gene-trap vector were used to amplify the vector insertion site for each clone, which was then compared to mouse genome sequence assemblies to localize the insertion with respect to the exons and introns of the gene. Gene disruption *in vivo* for gene-trap mutations was confirmed by a direct analysis of gene expression using RT-PCR. RNA was extracted from at least two tissues of wild-type (WT) and homozygous mutant mice using a bead homogenizer and RNAzol (Ambion, Austin, TX, USA) according to manufacturer's instructions. Reverse transcription was performed with SuperScript II (Invitrogen, Carlsbad, CA, USA) and random hexamer primers, according to the manufacturer's instructions. PCR amplification was performed with oligonucleotide primers complementary to exons flanking the insertion site.

Targeted or gene-trap mutations were generated in strain 129SvEv^{Brd}-derived ES cells. The chimeric mice were bred to C57BL/6J albino mice to generate F1 heterozygous animals. These progeny were intercrossed to generate F2 WT, heterozygous and homozygous mutant progeny. This generation was used for HTS phenotyping. On rare occasions, for example when very few F1 mice were obtained from the chimera, F1 heterozygous mice were crossed to 129SvEv^{Brd}/C57 hybrid mice to yield additional heterozygous animals for the intercross to generate the F2 mice. KO mice could not be generated for three genes, as heterozygous *Pstk* mice were infertile and, confirming published observations, KO of *Cask*[49] and *Dll4*[50] resulted in heterozygous lethality.

Lexicon's KO strategies for *Agpat2*, *Clcn7*, *Cldn18*, *Fam20c*, *Gnptab*, *Lrp5*, *Lrrk1*, *Sgpl1*, *Stk36*, *Tph1*, *Tph2* and *Wnt16* are provided in the publications of these phenotypes. KO strategies used to generate 4 077 of Lexicon's KO mouse lines are provided at the Taconic Farms website (http://www.taconic.com/KO). Supplementary Table S1 summarizes KO strategies for all 93 genes discussed in this review.

A total of 139 X-linked genes were KO'd, with bone data for 133 KOs reported. Male mice having an X chromosome gene KO'd are designated hemizygous. KO of two lines resulted in reduced viability and KO of four X-linked genes (*Ebp*, *Mmgt1*, *Porcn*, *Prps1*) resulted in hemizygous lethality. Data for 105 male hemizygous KO lines were analyzed. For 28 X-linked KOs DEXA data were analyzed for hemizygous and WT males plus homozygous female KO mice compared to age-matched WT female mice from the breeding colony. For 90 of these 105 KOs, data for only two male WT mice were available for DEXA calculations.

High-throughput screening assays

DEXA BMD was determined in 14-week-old mice anesthetized with 250 mg·kg^{-1} tribromoethanol given intraperitoneally using a GE/Lunar PIXImus scanner. For each KO line, mean body spine and femur BMD ratios for KO/WT littermates were calculated separately for both male and female mice, and then these male and female data were averaged to yield a normalized BMD value for each site. For most KO lines, four male KO (actual mean=4.2), two male WT (mean=2.2), four female KO (mean=4.2) and two female WT (mean=2.1) mice were analyzed. Lines with fewer than four KO mice or fewer than three WT mice were excluded. When there was an uneven distribution of male and female mice, normalized BMD values were weighted to account for the actual number of mice analyzed. Body vBMD was calculated by dividing body BMD by the square root of body bone area. Body BMD and vBMD were correlated but vBMD had a lower variation. Spine BMD, femur BMD and body BMC/lean body mass (LBM) ratio were also determined. BMD values for left and right femurs were averaged for the HTS, but left femur BMD alone was employed for secondary screens.

These DEXA scans also provided body fat and LBM data for our obesity phenotyping program. The body composition measurements were validated against carcass composition determined by chemical analysis.[51] A summary of the first 2 322 KO genes evaluated has been published[11], with identification of *Ksr2* as a novel hyperphagic obesity gene. For most KO lines, architectural parameters of LV5s and femurs from four male KO (actual mean=4.1) and two male WT (mean=2.1) mice were determined at 16 weeks of age using a Scanco Medical μCT40 (Brüttisellen, Switzerland). Trabecular bone within the vertebral body was evaluated.

MicroCT X-ray voltage and current were 55 keV and 145 μA, respectively. Isotropic voxel dimensions for the HTS scans were 16 μm for LV5s and 20 μm for femurs, but higher resolution scans (8 μm voxel dimensions) were often employed for many of the secondary screen analyses. Vertebral body trabecular BV/TV, thickness and number were analyzed in LV5 scans and midshaft cortical thickness and total area (a surrogate for bone diameter) were analyzed in femur scans. Scans of 10 random LV5s with a range of trabecular bone mass showed the expected linear decrease in BV/TV values as the microCT threshold value was increased. After consultation with Scanco Medical, a threshold value of 240 was employed for all scans.

To generate high-throughput microCT scans, we engaged a machinist to construct Plexiglas inserts to hold multiple bones and fit snuggly inside the μCT40 sample holders. These inserts held 48 LV5s (12 rows of 4 bones per row) for overnight scanning, allowing four LV5s to be scanned simultaneously. Separate inserts held 18 femurs (three rows of six bones per row) allowing six femurs to be scanned simultaneously in 10 min. Photographs of these inserts are provided in Figure 1.

Histological examinations of bone were included as part of a comprehensive analysis of multiple tissues.[22] The HTS analyses examined femur, tibia, sternum and nasal turbinates. Additional bones (vertebrae, calvarium and forelimbs) were examined in follow-up studies for selected KO mice having skeletal phenotypes in the HTS.

Advanced bone phenotyping assays

Deciding which KOs showing potential skeletal phenotypes in the primary HTS merited advancement to secondary screening involved both statistical and judgmental considerations. Given that multiple parameters were measured from a small numbers of mice, strict statistical tests were not employed. Knowing the means and standard deviations of each parameter, we sought consistency among the various DEXA and microCT values. Values for KO mice were compared to both littermate WT controls and historical WT data.

Additional methods, such as ovariectomy, daily subcutaneous teriparatide treatment, measurement of serum levels of PINP as an index of bone formation[52] and bone breaking strength, all involved standard protocols. Biomechanical parameters were measured at Numira Biosciences (previously SkeleTech, MDS Pharma Services and Ricerca Biosciences, Salt Lake City, Utah, USA) using standard procedures for LV5 compression and femur shaft four-point bending. Body CT scans were performed using an ImTek scanner (Siemens, Munich, Germany). Three-dimensional images were reconstructed using the Feldkamp algorithm with ImTek 3D RECON software.

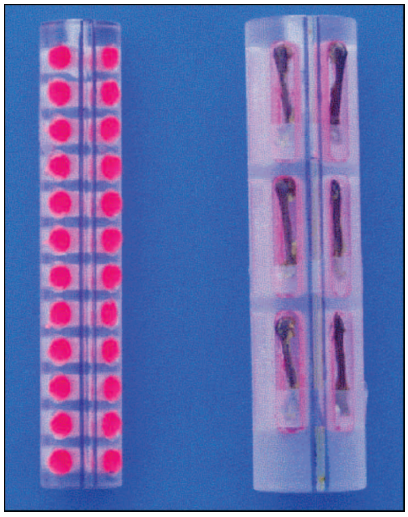

Figure 1. Photograph showing Plexiglas plastic inserts employed to align LV5 vertebral bodies (left) and femurs (right) inside sample holders for the Scanco μCT40 microCT scans. The red dots indicate placement of LV5s, with 12 rows of 4 columns. The lack femurs indicate placement of femurs, with three rows of six columns. Bones are fixed in place by adhering soft tissue and removable tape around the outside of the insert.

Lexicon developed two neutralizing mouse antibodies to Dickkopf 1 (DKK1). Mice were immunized with purified mouse DKK1 protein produced in HEK293 cells. Total RNA was obtained from the spleens of immunized mice and a phage library displaying FAb fragments was constructed. Phage displaying DKK1-specific FAbs were selected on immobilized DKK1 protein and monoclonal FAbs were generated in *Escherichia coli*. The specificity of FAbs for DKK1 was confirmed by ELISA. Chimeric proteins composed of combinations of the N-terminal leader/CYS1 domain and the C-terminal CYS2 domain/tail of DKK1, DKK2 and DKK4 were produced by transient transfection in HEK293 cells and used to map FAb epitopes. The ability of FAbs to inhibit the activity of DKK1 was determined using the CellSensor® LEF/TCF-bla FreeStyle™ 293F reporter cell line (Invitrogen, Grand Island, New York, USA) in the presence of exogenous Wnt3a (R&D Systems, Minneapolis, Minnesota, USA) and exogenous DKK1 protein. The ability of FAbs to inhibit binding between DKK1 and LRP6 was determined in an ELISA-based binding assay utilizing purified DKK1 protein and purified LRP6 ectodomain-Fc fusion protein (R&D Systems). Based on their ability to inhibit DKK1 function *in vitro* and their binding mapping to distinct domains of DKK1, two FAbs were selected for conversion to full length mouse IgG1 antibody, production from CHO cells, and testing *in vivo*. Full-length antibody affinities for mouse and human DKK1 were measured using a Biacore 3000 (GE Healthcare, Pittsburgh, Pennsylvania, USA) with DKK1 in the solution phase.

Mouse husbandry

Mice were housed in micro-isolator cages within a barrier facility at 24 ℃ on a fixed 12-h light and 12-h dark cycle and were provided *ad libitum* acidified water and Purina rodent chow # 5001 (Purina, St Louis, MO, USA). Procedures involving animals were conducted in conformance with Lexicon Pharmaceuticals' Institutional Animal Care and Use Committee guidelines, that are in compliance with state and federal laws and the standards outlined in the Guide for the Care and Use of Laboratory Animals (National Research Council, 2011). Quarterly sentinel surveillance showed no evidence of pathogenic rodent viruses, *Mycoplasma* or *Helicobacter* species in the Lexicon Pharmaceuticals source colonies.

RESULTS

High-throughput screen data

Viable mice from 3 762 distinct KO genes were evaluated by various combinations of DEXA (*N*=3 651), microCT LV5 trabecular bone (*N*=3 399) and/or microCT midshaft femur cortical bone (*N*=3 366) scans. All three analyses were performed on 87% (*N*=3 255) of the KO lines. A Venn diagram showing the overlap of these assays is presented in Figure 2. Sixty-four percent of gene KOs were generated by homologous recombination and 36% by gene-trap technologies. These numbers include only KO lines for which viable mice survived through 14 weeks of age. Bone phenotypes were also identified by DEXA and microCT scans in heterozygous mutant *Dkk1* mice and from two KO lines with reduced viability (*Klotho* and *Sgpl1*). Histologic examinations identified detrimental bone phenotypes in seven KO lines that did not survive until 12 weeks of age (*Fgf23*, *Nppc*, *Npr2*, *Ostm1*, *Slc25a1*, *Slc30a10*, *Sumf1*).

Beyond these KO lines examined, additional KO lines were generated but are not included in this count. Of these, embryonic or neonatal lethality was observed in over 840 KO lines while the number of WT and/or KO mice generated for 41 KO lines was considered too low to provide adequate data for HTS bone measurements (see above) and were thus excluded from analyses. Three KO lines were generated prior to purchase of our DEXA scanners. Thus, mouse KOs were generated for more than 4 650 genes.

Figure 3 presents histograms of the gene KOs showing means, s.d.s and normal distribution values for DEXA vBMD, LV5 trabecular bone BV/TV and midshaft femur cortical thickness. For illustration, selected HTS values of mouse KOs having bone phenotypes are indicated. HTS data for all genes of interest are provided in the tables and text below.

HTS data for Lexicon's published KOs

The HTS (Table 1) clearly identified skeletal phenotypes for *Cldn18*, *Fam20c*, *Lrp5*, *Lrrk1*, *Sgpl1*, *Sost and Wnt16* and comprehensive follow-up studies for each of these KO lines have been published.

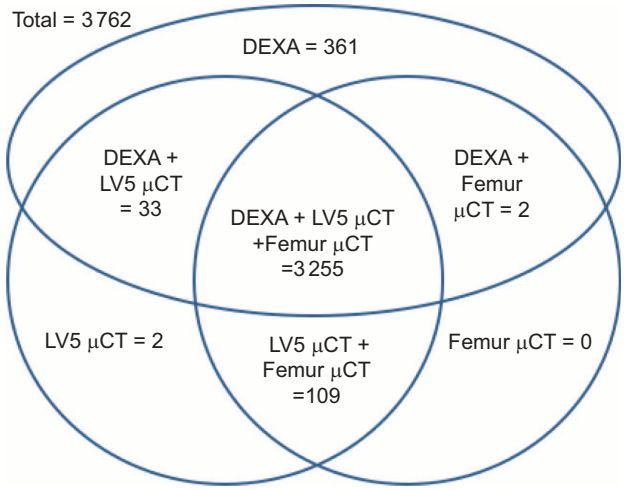

Figure 2. Venn diagram showing the numbers of KO lines undergoing HTS analyses for DEXA, LV5 microCT and femur shaft microCT.

The 24 mammalian claudin proteins are components of membrane tight junctions regulating permeability between cells.[53] Although *Cldn18* is highly expressed in osteoblasts,[40,54] bone cells are believed to contain gap junctions but not tight junctions.[55] Consistent with high expression of Cldn18 in gastric cells and in agreement with a previous report,[56] Lexicon's *Cldn18* KO mice had severe gastritis.[40] Osteoclast activity was increased with KO of *Cldn18*, resulting in low bone mass.[40] *Cldn18* KO mice fed a high calcium diet remained osteopenic, demonstrating an intrinsic osteoclast defect[57] and not a secondary osteoclastic response to a possible low intestinal calcium absorption from reduced gastric acid secretion.

Fam20c KO mice grew poorly after weaning (LBM is 53% of normal), having dental lesions, hypophosphatemic rickets and greatly elevated serum levels of FGF23.[42] Identical phenotypes were observed in an independent mouse KO.[58] Human mutations result in Raine syndrome with neonatal lethality the usual outcome.[59] During the time these mouse KOs were being characterized two independent groups demonstrated that FAM20C is a Golgi kinase that phosphorylates proteins undergoing secretion.[60–61] FAM20C has recently been shown to phosphorylate FGF23 at serine 180, inhibiting *O*-glycosylation of

Table 1. Primary screen data for seven gene KOs published by Lexicon

Gene	Analysis	N	vBMD/%	Spine BMD/%	Femur BMD/%	LV5 TBV/%	Femur CT/μm
Control Data	HTS	—	100	100	100	16	246
Cldn18	HTS	12	88	78	80	13	201
Fam20c	HTS	12	84	60	58	9	99
Lrp5	HTS	12	84	82	77	15	226
Lrrk1	HTS	12	133	171	174	NM	NM
Sgpl1	HTS	10	97	74	72	52	NM
Sost	HTS	12	129	146	135	43	356
Wnt16	HTS	12	98	96	106	19	201

Due to reduced viability, *Sgpl1* KO and WT littermate mice were examined between 3 and 6 weeks of age. HTS=high-throughput primary screen; NM=not measured.

threonine-178 and thereby promoting proteolysis to inactive N- and C-terminal fragments.[62] FAM20C also phosphorylates casein, BMP15 and SIBLING bone matrix proteins.

As established by other groups, KO of *Lrp5*[63–65] and *Sost*[66–67] result in low and high bone mass (HBM), respectively. In agreement with an independent *Lrp5* KO mouse study[68] and a recent human trial examining a patient with a *LRP5* mutation,[69] Lexicon showed that *Lrp5* KO mice respond to the anabolic actions of teriparatide.[26] Lexicon demonstrated that male *Sost* KO mice continue to gain cortical bone through 2 years of age, with male and female KO mice losing bone following castration.[27] These *Sost* KO mouse data will be presented separately. Lexicon also contributed to a multi-institution study showing that Lrp5 acts locally in osteoblasts to influence bone mass,[70] arguing against systemic actions of gut-derived serotonin on bone mass.[71] *Lrp5* KO mice generated independently at Lexicon and the Max Delbrück Center for Molecular Medicine (Germany) did not show any disturbances in serotonin metabolism.[70]

Patients having loss-of-function mutations in *LRP5* and *Lrp5* KO mice have eye vascularization defects.[63] KO of any of four distinct genes in mice leads to failure of retinal hyloid vessels to regress during development: the secreted proteins *Ndp*[72–73] and *Wnt7b*,[74] and the coreceptors *Frd4*[72] and *Lrp5*.[64,75] Not described in our *Lrp5* publication[26] is the fact that Lexicon's KO mice have these ocular defects. Histologic examination (Supplementary Figure S1a) showed that photoreceptors, inner retinal cells and ganglion cells were distributed in three cellular layers, the outer nuclear layer, inner nuclear layer and ganglion cell layer, respectively, in WT retinas. Synaptic connections among these cells occur in the outer plexiform layer and inner plexiform layers. In *Lrp5* KO mice, the vitreous, which is clear in healthy retinas, contained protein exudates (asterisks) and the inner nuclear layer was disrupted by large infiltrating blood vessels (arrowheads) that apparently failed to disperse, but formed a deep capillary plexus. Lexicon has also confirmed and extended findings of similar ocular vascularization defects in *Fzd4* KO mice.[76]

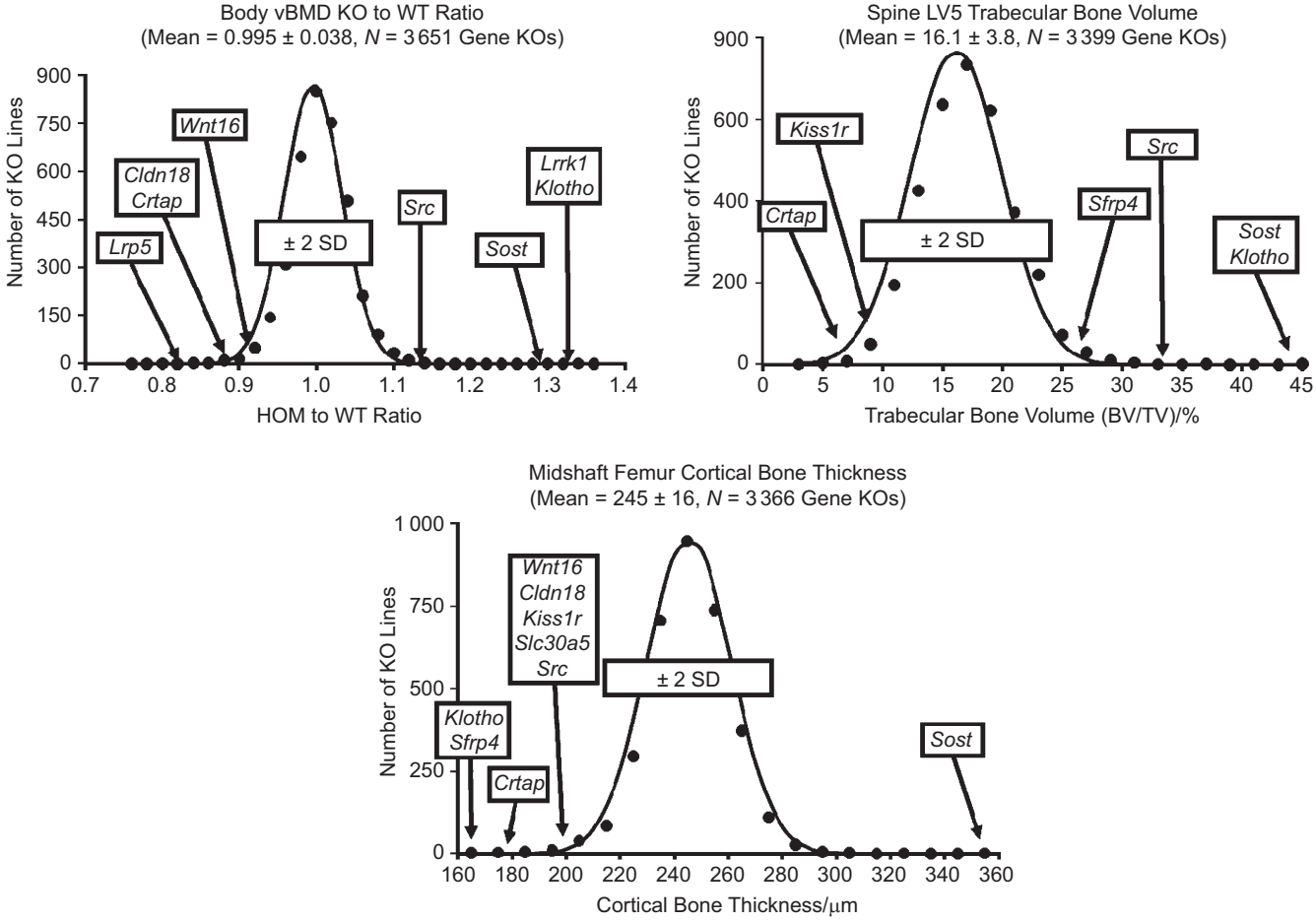

Figure 3. Histograms showing distributions of vBMD (N=46 228 mice), LV5 Tb BV/TV (N=13 979 mice) and midshaft femur cortical thickness (N=13 845 mice) HTS values for all gene KOs examined, with s.d. indicated. Lines show normal distributions for the calculated means and s.d.s. HTS data for selected genes having clear bone phenotypes are indicted by arrows. s.d., standard deviation.

LRRK1 is a serine/threonine kinase containing three ankyrin repeat domains, seven leucine-rich repeat domains, a Roc GTPase domain, a COR domain and a kinase domain.[77] Mutations in the related *LRRK2* gene are the most common genetic cause of Parkinson's disease and since these mutations often result in enhanced kinase activity, drug development efforts are underway to discover small molecule inhibitors of this target. Lexicon's *Lrrk1* KO mice (which lack the GTPase domain as a result of targeted deletion of exons 16–19) have severe osteopetrosis resulting from dysfunctional osteoclasts.[39] A second *Lrrk1* KO line (C57BL/6-*Lrrk1*^{tm}[1.]^{1Mjff}/J, lacking exons 24–29 which encode the kinase domain) and Lrrk1 KO rats (LEH-Lrrk1^{em1sage}[−/−]) are available from the Michael J. Fox Foundation[78] through Jackson Laboratories (Bar Harbor, Maine, USA) and SAGE Labs (Boyertown, Pennsylvania, USA), respectively. C57BL/6-*Lrrk1*$^{tm1.1Mjff}$/J KO mice suffer from neonatal lethality and reasons for phenotype differences resulting from the two different KO strategies are unclear.

Sphingosine-1-phosphate (S1P), a signaling phospholipid produced from ceramides by the actions of ceramidase and sphingosine kinase, is a ligand for five GPCR receptors (S1P1 through S1P5) and is inactivated by S1P lyase (SGPL1). Among other actions, S1P inhibits migration of T lymphocytes from thymus and lymph nodes into the circulation and therefore pharmacological analogues of S1P (fingolimod) or treatments that increase endogenous S1P levels are immunosuppressive. Plasma S1P levels are elevated in postmenopausal women with vertebral fractures.[79] Several laboratories, including Lexicon,[45] have shown that global KO of *Sgpl1* results in sickly mice having lymphopenia and markedly reduced lifespan. Lexicon's comprehensive histological examination showed lung, heart and urinary tract lesions, along with osteopetrosis. Osteoclasts are plentiful but have increased cytoplasmic volume and show increased incidence of degeneration and apoptosis. Thickened trabecular bones suggest that osteoclasts are not fully functional. Complementing the histological bone sections demonstrating osteopetrosis,[45] Figure 4 shows microCT images with greatly increased femoral trabecular bone content in KO mice. In addition to influencing osteoclast function, S1P is also produced by osteoclasts and stimulates bone formation by osteoblasts.[44,80] Complete genetic rescue of the non-lymphoid lesions, including osteopetrosis, was achieved in transgenic mice having mouse *Sgpl1* replaced by human *SGPL1*. These *humanized* mice have spleen SGPL1 enzyme activity 17% of normal and are healthy, but continue to exhibit lymphoid defects.[45] Pharmacological inhibition SGPL1 in mice[81] and humans[82] increased circulating S1P levels and decreased circulating T-lymphocytes.

Lexicon's *Wnt16* KO mice are healthy with normal bone length and trabecular bone mass, but reduced cortical bone diameter and thickness[37–38] and fail to add new periosteal bone after mechanical loading.[83] Additional data for Lexicon's *Wnt16* KO mice are provided in Supplemental Table S2, as part of the *Wnt16*/*Sfrp4* double KO (DKO) study described below. These Lexicon *Wnt16* KO mice were on a mixed (hybrid) C57BL/6J–129SvEv genetic background but another group found that *Wnt16* KO mice on a C57BL/6J genetic background developed spontaneous fractures associated with reduced thickness but normal diameter cortical bone.[84] Thus, a cortical bone deficit occurs in both mouse lines with mechanistic differences in the development of skeletal phenotypes. Periosteal bone formation is reduced in hybrid mice but normal in C57BL/6J mice, with endocortical bone resorption near normal in hybrid mice but increased in C57BL/6J mice.

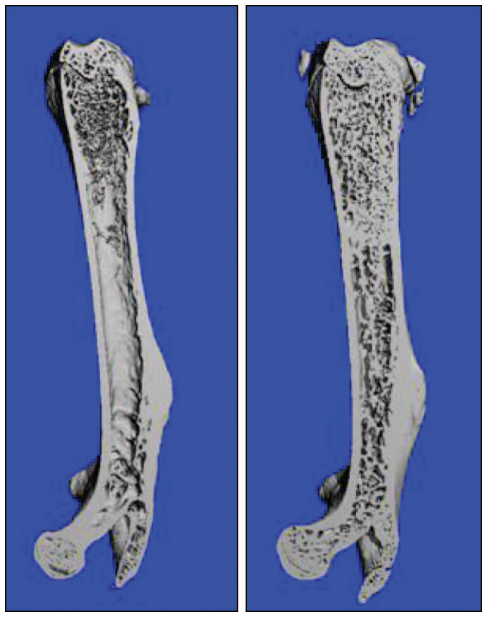

Figure 4. MicroCT scans of femurs from WT (left) and *Sgpl1* KO (right) mice.

KOs with HTS data only—confirming published KOs

Lexicon's HTS confirmed previously published skeletal phenotypes of mouse KOs for numerous genes. These successful confirmations demonstrate the power of the HTS measurements and provide confidence that there were minimal false negatives when screening for novel genes affecting bone mass. Table 2 presents HTS data for *Cebpb*, *Crtap*, *Enpp1*, *Kremen1*, *Kremen2*, *Klotho* *Slc39a13* and *Src*. Since these established skeletal phenotypes are unambiguous, no bone analyses were performed on additional cohorts of mice.

Four groups have shown that the transcription factor *Cebpb* (CCAAT/enhancer binding protein beta) KO mice

Table 2. Primary screen data Cebpb, Crtap, Enpp1, Klotho, Kremen1, Kremen2, Neo1, Pstn, Slc39a13 and Src

Gene	Analysis	*N*	vBMD/%	Spine BMD/%	Femur BMD/%	LV5 TBV/%	Femur CT/μm
Control Data	HTS	—	100	100	100	16	246
Cebpb	HTS	12	87	79	85	12	248
Crtap	HTS	12	89	85	90	7	180
Duoxa2	HTS	12	103	108	85	NM	NM
Enpp1	HTS	12	95	90	78	5	191
Klotho	HTS	7	132	122	68	44	165
Kremen1	HTS	12	104	104	98	17	258
Kremen2	HTS	12	98	101	97	12	244
Neo1	HTS	12	90	77	86	11	212
Pstn	HTS	12	93	79	88	12	250
Slc39a13	HTS	12	87	92	91	5	211
Src	HTS	10	114	128	125	33	208

Due to reduced viability, *Klotho* KO and WT littermate mice were examined at 10 weeks of age. HTS=high-throughput primary screen. NM=not measured.

are small with reduced bone mass[85–88] and these observations were confirmed in Lexicon's KO mice as LBM was 82% of normal and BMD values were reduced.

Cartilage-associated protein is an enzyme that hydroxylates proline at carbon-3 in collagen and mutations cause osteogenesis imperfecta with connective tissue defects in humans and mice.[89–90] *Crtap* KO mice had reduced viability with low BMD and microCT parameters. Nasal turbinates (Supplementary Figure S1b) were fragile during handling and showed increased basophilia, diffuse thinning and numerous discontinuities in the bone plates.

Dual oxidation maturation factor 2 (DUOXA2) is a transmembrane protein required for plasma membrane localization of the hydrogen peroxide generating enzyme DUOX2. Hypothyroidism results from mutations in *DUOX2* and *DUOXA2* in humans[91] and KO of *Duox2*[92] or DKO of *Duoxa1/Duoxa2*[93] in mice. As expected, *Duox2* KO mice are dwarfs with low femur BMD.[94] Lexicon's *Duoxa2* KO mice showed clear signs of hypothyroidism, including hypertrophic TSH-secreting cells in the pituitary, goitrous thyroid, growth retardation, bone epiphyseal flattening, reduced medullary area, altered articular surfaces and increased numbers of brown fat adipocytes containing large fat droplets. HTS DEXA scans showed reduced LBM (57% of normal) and femur BMD (85% of normal), but due to small body size, body vBMD and spine BMD were normal. As expected, body BMC (69% of normal) and BMD (90% of normal) were greatly reduced. In agreement with published data,[95] KO of *Duox1* did not result in hypothyroidism (data not shown).

Mice with the ectonucleotide pyrophosphatase/phosphodiesterase family member 1 (*Enpp1*) gene KOed[96] or disrupted by spontaneous mutation[97] or ENU mutagenesis[98–99] have ectopic calcifications. Lexicon's *Enpp1* KO mice had low bone mass and modest hypophosphatemia (5.2 ± 0.2 *versus* 7.2 ± 0.3 mg·dL^{-1}, $P=0.004$) with ankylosing intervertebral and peripheral joint hyperostosis, multifocal calcification of arteries, ligaments, tendons and articular cartilage and the splenic capsule.

KLOTHO is a FGFR coreceptor that binds FGF23.[100–101] Confirming published data, Lexicon's *Klotho* KO mice had poor growth and few survived past 10 weeks of age. The bone phenotype was unusual as high trabecular bone mass coexisted with low cortical bone mass[102] and these defects were rescued by simultaneous deletion of PTH.[103] These skeletal phenotypes resulted in elevated values for body vBMD, spine BMD and spine trabecular BV/TV, but reduced values for femur BMD and cortical thickness. A histological section of a femur from a KO mouse is shown in Supplementary Figure S1c.

KREMEN1 and KREMEN2 are single transmembrane proteins that bind to DKK1 and LRP6, but the exact mechanism of KREMEN action is unclear. We did not observe any obvious skeletal phenotypes in our HTS screens for *Kremen1* and *Kremen2* KO mice and this finding was independently confirmed in mice examined at 12 weeks of age.[104] Interestingly, double KO mice with disruptions of both *Kremen1* and *Kremen2* genes are viable and have high trabecular bone mass resulting from elevated bone formation.[105] However, this same group subsequently showed that *Kremen2* has high bone expression, osteoblast-specific overexpression of *Kremen2* produces low bone mass and that *Kremen2* KO mice have elevated trabecular bone mass at 24 weeks of age.[105]

Neogenin is a cell surface protein modifying BMP receptor association with membrane lipid rafts and *Neo1* KO mice have abnormal chondrocyte maturation and endochondral bone growth.[106] Lexicon's KO mice had low bone mass parameters in the HTS screen and growth plate hypoplasia histologically (Supplementary Figure S1d).

Periostin is a secreted matricellular protein highly expressed in the periosteum.[107–108] *Postn* KO mice have low bone mass,[109–110] a minimal bone formation response to exercise and axial compression and increased bone fatigue damage in response to loading.[111] Reduced bone mass was observed in Lexicon's HTS screen.

SLC39A13 is a zinc transporter. Gene disruption is associated with multiple abnormalities, including low bone

mass, in KO mice,[112] and the spondylocheiro dysplastic form of Ehlers–Danlos syndrome in humans.[113] Lexicon's HTS confirmed growth retardation (LBM is 73% of normal), a generalized low bone mass phenotype and dysplasia of the epiphyseal growth plate cartilage. The cartilage was thickened (2–3 times normal) and disorganized with increased interchondrocyte matrix material of a loose fibrillar appearance. The cytoplasm of mature chondrocytes was distended by large eosinophilic granules. KO mice also exhibited modest thickening of the articular cartilage (Supplementary Figure 1e).

Src was first identified as an osteopetrosis gene in 1991.[126] Lexicon's KO mice were small (LBM was 81% of normal) with high values for BMD and trabecular bone by microCT. Cortical bone thickness was low. Histologic examination showed osteopetrosis and dysplasia of incisor teeth. Bones were characterized by medullary cavities (Supplementary Figure S1h) filled with trabecular bone and thinning of the cortical bone. Nasal turbinate bones were distorted and up to five times thicker than normal.

The DEXA, microCT and histological assays used in HTS at Lexicon accurately confirmed these nine established skeletal KO phenotypes (and normal bone mass in *Kremen1* and *Kremen2* KO mice). In addition, three KO lines having severe bone phenotypes (*Fgf23*, *Ostm1 and Nppc*) but not surviving to undergo DEXA and microCT scans were confirmed histologically.

FGF23 is secreted by osteocytes to stimulate renal phosphate excretion and calcitriol synthesis. *Fgf23* KO mice have a maximum lifespan of 13 weeks, are hyperphosphatemic and have multiple skeletal defects.[114] Lexicon's KO mice were small and sickly and euthanized at 6 weeks of age without serum P determination. Histologically, defective mineralization of bone was observed, characterized by retention of cartilage cores in cortical and trabecular bone in long bones and thickening of turbinate and calvarial bones, as well as apposition of woven bone on the endosteal surfaces of the diaphysis. Although osteoblasts in regions with normally high bone turnover had a normal appearance, the overwhelming majority of osteoblasts in other areas were abnormal. The abnormal osteoblasts were up to fivefold normal size and frequently filled the intertrabecular marrow spaces. The cytoplasm of affected osteoblasts and osteocytes was distended by abundant basophilic material, presumably matrix proteins. Mineralization was consistently present in the kidney and duodenum and regions in the aorta, trachea and stomach. Ectopic mineralization in the kidney was relatively mild and limited in distribution to proximal tubules located near arcuate vessels.

Mutations in *OSTM1* are responsible for osteopetrosis in humans and the spontaneous grey lethal osteopetrotic mouse.[115–116] This gene codes for a transmembrane protein that forms the beta subunit of the CLNC7 chloride transporter, mutations in which also lead to osteopetrosis.[117] Lexicon's *Ostm1* KO mice were small and failed to thrive with a grey coat color and no teeth. Microscopic analysis revealed retinal degeneration, reactive astrogliosis (hypertrophy with inclusion bodies), neuronal necrosis and osteopetrosis. The medullary cavities of all long bones, vertebrae and sternebra were filled with trabecular bone (Supplementary Figure S1f). Osteoclast numbers were increased and in some areas there were degenerating and necrotic osteoclasts. Osteoblasts were also numerous, although they tended to be elongated and fibroblastic. Bones in the skull, nasal trabecula and epiphyses of long bones contained abundant loosely woven bone and trabecula.

C-type natriuretic peptide (CNP, gene symbol *NPPC*) stimulates longitudinal bone growth though natriuretic peptide receptor B (NPR2). KO of mouse *Nppc*[118] and three spontaneous mouse (*cn*, *slw and lbab*) mutations[119–121] all result in dwarfism. The involvement of NPR2 in growth plate development is shown by mutations in humans and mice,[122] with a gain-of-function mutation in humans leading to tall stature.[123] Most *Npr2* KO mice at Lexicon died young and the few survivors were small and sickly. Achondroplastic dwarfism, resulting from laminar hypoplasia of the epiphyseal cartilage, was confirmed by histological examination. Limb bones had nearly normal diameters but were markedly shortened, especially in comparison to the craniofacial bones formed by intramembranous ossification. Zones of resting and proliferating cartilage had nearly normal thickness but there was marked thinning of the zones of hypertrophic and degenerating chondrocytes. The zones of calcification that are normally composed of cartilage cores lined by hypertrophic osteoblasts were almost entirely absent (Supplementary Figure S1g). There was severe dental malocclusion due to unequal growth rates of the calvarium and mandible.

Osteocrin is a secreted protein with homology to A- and B-type natriuretic peptides. Osteocrin binds to natriuretic peptide receptor C (NPR3), a clearance receptor for natriuretic peptides, and thereby increases local concentrations of these natriuretic peptides. An ENU-induced point mutation in the mouse *Npr3* extracellular domain, presumably inhibiting CNP clearance, results in elevated longitudinal bone growth.[124] Mice with transgenic overexpression of osteocrin in osteoblasts, expected to inhibit CNP clearance, have normal bone mass but elongated tails and femurs[125]. Lexicon's *Ostn* KO mice had normal bone mass in the HTS (data not shown). Femoral and tibial lengths in both male and female mice determined from DEXA scans were unaltered ($P>0.6$, data not shown). Thus, CNP signaling in the bone growth plate appears to be

unaffected by disruption of osteocrin, but stimulated by both elevated osteocrin levels and disruption of the NPR3 clearance receptor.

Genes involved in WNT signaling

Great interest in the roles of Wnt signaling on bone mass followed the 2001/2002 discoveries that various *LRP5* and *SOST* gene mutations in humans are responsible for dramatic alterations in patients with osteoporosis pseudoglioma, the HBM phenotype, sclerosteosis and van Buchem's disease. Along with Frizzled receptors, LRP5 and LRP6 are coreceptors for the 19 WNT ligands with sclerostin (coded by the SOST gene) blocking WNT binding to LRP5/6. Since inactivating *LRP5* (osteoporosis pseudoglioma syndrome) and *LRP6*[127–128] mutations decrease bone mass, whereas activating *LRP5* mutations (HBM phenotype) and mutations disrupting *SOST* expression (sclerosteosis and van Buchem's disease) increase bone mass, WNT signaling must activate bone formation. As described above, KO of *Lrp5* and *Sost* in mice produce the identical skeletal phenotypes as the human inactivating mutations. Furthermore, transgenic mice with *Lrp5* activating mutations have extremely HBM.[70,129]

WNT signaling can also be inhibited by DKKs that bind LRP5/6 and Secreted frizzed-related proteins (SFRPs) that bind WNTs. As is the case with sclerostin, reducing levels of DKKs and SFRPs in bone should remove inhibitors of WNT signaling, thereby presumably increasing bone mass. Support for this idea was available in the original HBM publication describing the LRP5 activating mutation, which in cells eliminated the inhibitory actions of DKK1.[130] The key role of WNT signaling in bone prompted us to examine KO mice for all four *Dkk*s, five *Sfrp*s and *Wif1* (Table 3). KO of *Dkk1* leads to embryonic lethality, but mice with disruptions of the other eight genes were viable.

HBM is observed in *doubleridege* mice having a spontaneous mutation leading to reduced DKK1 expression,[131] *Dkk1* heterozygous mutant mice[132] and *Dkk1* homozygous KO mice generated on a *Wnt3* heterozygous mutant background.[133–134] Osteoblast-specific overexpression of *Dkk1* in mice leads to severe osteopenia.[135] Lexicon confirmed observations of HBM in heterozygous *Dkk1* KO mice. These and other observations prompted several groups, including Novartis,[136] Merck,[137–138] Amgen,[139] Eli Lilly[140] and Lexicon, to develop anti-DKK1 neutralizing antibodies for potential therapeutic treatment of osteoporosis and other bone diseases, particularly multiple myeloma.[141]

Lexicon's DKK1 Antibody #1 recognizes an epitope in the C-terminal half of DKK1 that prevents DKK1 binding to LRP6. Antibody #2 recognizes an epitope in the N-terminal half of Dkk-1 that does not affect Dkk1 binding to LRP6. Identical anti-DKK1 epitope specificities for LRP6 binding have been reported by Amgen.[142] Both Lexicon antibodies have potencies below 500 pM as determined by binding affinities to human DKK1 (416 pM for Ab #1 and

Table 3. Primary and secondary screen data for WNT antagonists

Gene	Analysis	*N*	vBMD/%	Spine BMD/%	Femur BMD/%	LV5 TBV/%	Femur CT/μm
Control Data	HTS	…	100	100	100	16	246
Dkk1 (HETs)	HTS	12	100	103	105	29	254
	SS	23	112	136	108	29	267
Dkk2	HTS	12	97	106	97	19	242
	SS	28	109	112	108	20	252
Dkk3	HTS	12	100	104	102	18	255
	SS	42	96	93	98	16	255
Dkk4	HTS	13	102	94	104	16	246
	SS	19	99	104	100	20	268
Sfrp1	HTS	12	97	90	97	18	249
	SS	30	100	107	104	22	277
Sfrp2	HTS	12	102	101	102	21	253
	SS	23	99	100	101	NM	NM
Sfrp3	HTS	12	98	96	106	16	245
	SS	17	100	105	99	16	264
Sfrp4	HTS	12	93	95	88	26	167
	SS	39	93	98	93	30	159
Sfrp5	HTS	12	103	96	95	13	242
	SS	43	102	103	101	22	258
Wif1	HTS	12	100	100	94	19	252
	SS	28	101	91	100	NM	NM
Wnt10a	HTS	12	98	100	98	17	243
Wnt10b	HTS	12	92	97	92	14	236

Mouse ages in the secondary screens were 23 weeks for *Dkk1*, 14 and 28 weeks for *Dkk2*, 42 to 64 weeks for *Dkk3*, 19 to 29 weeks for *Dkk4*, 52 weeks for *Sfrp1*, 7 weeks for *Sfrp2*, 24 weeks for *Sfrp3*, 15 weeks for *Sfrp4*, 16 to 21 weeks for *Sfrp5*, and 20 to 30 weeks for *Wif1*. HTS=high-throughput primary screen; SS=secondary screen; NM=not measured.

347 pM for Ab #2) and mouse Dkk1 (128 pM for Ab #1 and 233 pM for Ab #2) and IC50 values (270 pM for Ab #1 and 370 pM for A b#2) in a mouse cell-based assay employing Wnt3a as a stimulator of Wnt signaling.

Three preliminary studies examining these two antibodies in adult male mice (>12 weeks of age) at weekly doses of 3–30 mg·kg^{-1} for 6 or 12 weeks all provided evidence of bone efficacy (data not shown). Since DKK1 expression in rat bone declines with age,[143] we performed a fourth study of 4 weeks duration in male mice starting at 4 weeks of age. Antibody #1 and antibody #2 were each given subcutaneously weekly at doses of 30 mg·kg^{-1}. A negative control group of mice was treated similarly with a control antibody. A positive control group of mice was treated at the start of the study with a single subcutaneous dose of 50 μg·kg^{-1} zoledronate to inhibit bone resorption.

Treatment with antibody #2 and zoledronate increased spine and femur BMD, and cancellous BV/TV in the LV5 vertebral body and distal femur metaphysis (Figure 5). Focusing on the LV5 vertebral body, antibody #2 treatment increased trabecular thickness but not trabecular number, whereas zoledronate treatment increased trabecular number but not trabecular thickness. This differential mechanism of cancellous bone gain is consistent with proposals that DKK1 inhibition acts to increase bone formation but zoledronate treatment acts to block bone resorption. Treatment with antibody #1 consistently showed trends to increase bone mass but this antibody was clearly inferior to antibody #2.

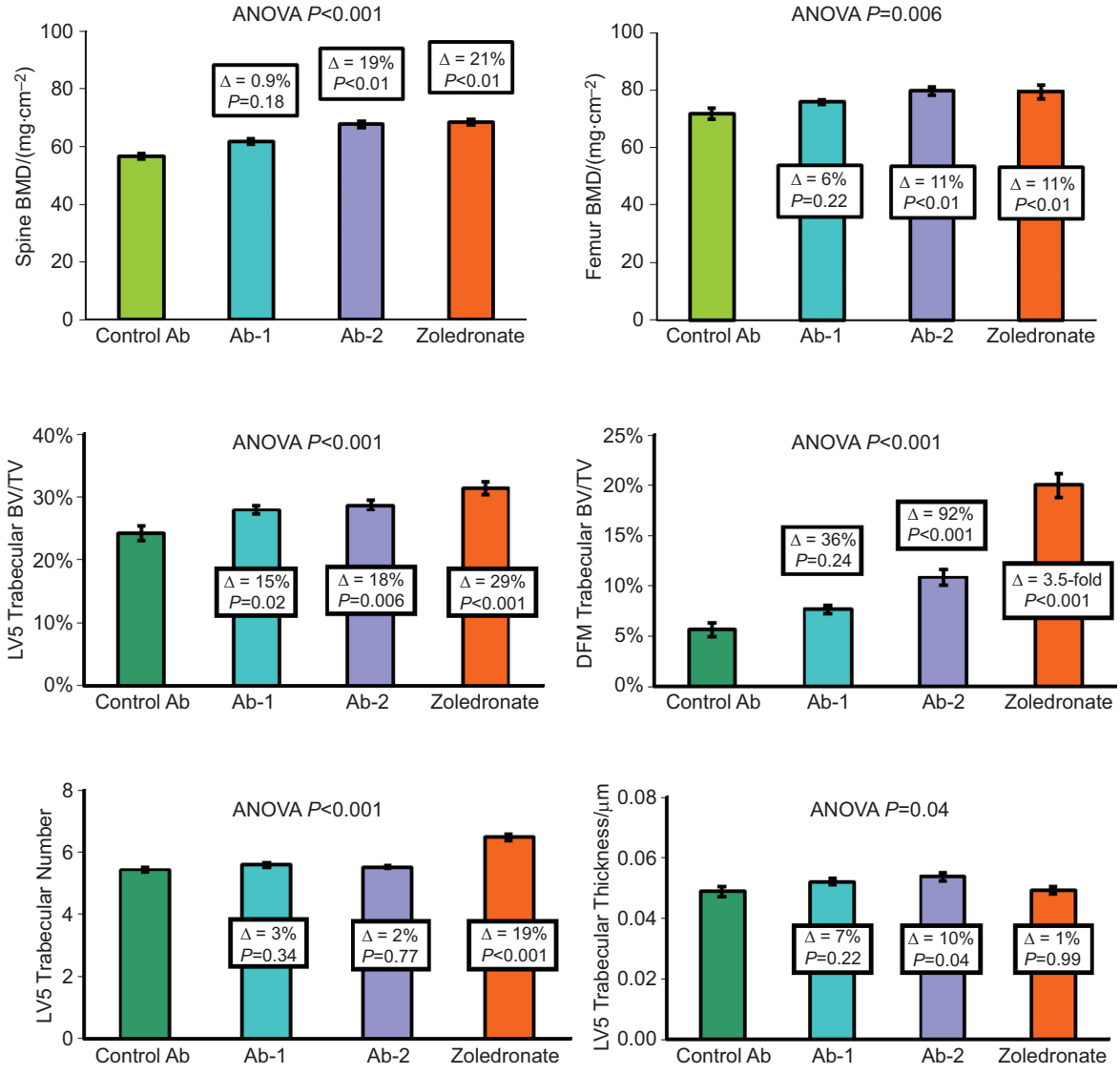

Figure 5. DKK1 antibody treatment in young mice. Data are means±s.e.m. for 10 mice per group treated between 4 and 8 weeks of age with antibody doses of 30 mg·kg^{-1} weekly or a single 10 μg·kg^{-1} zoledronate dose. Statistical evaluation involved ANOVA followed by Dunnett's test for multiple comparisons.

In agreement with previous reports,[144–145] Lexicon's *Dkk2* KO mice had numerous ocular abnormalities, including a lack of Harderian glands and malformed eyelids. The cornea and sclera contained sebaceous glands and hair follicles with multifocal keratitis and ulceration and fibrosis of the collageneous stroma. Although *Dkk2* KO mice have a normal skeletal architecture, their bone contains an excess of unmineralized osteoid.[146] Lexicon's KO mice had normal, or even slightly elevated, BMD. Undecalcified bone sections were not examined and therefore the excess osteoid phenotype was not evaluated. We rescanned eight WT and eight KO midshaft femurs at the highest microCT resolution possible (6 μm voxel size) and did not observe any hypomineralization of cortical bone, as material BMD was unaffected (0.7% higher with $P=0.27$) in bones from *Dkk2* KO mice. No gross skeletal phenotypes were previously detected in *Dkk3* KO mice[147] and Lexicon did not observe any bone abnormalities in the HTS.

Several groups generated viable *Sfrp2*, *Sfrp5*[148–149] KO or ENU-mutant *Sfrp5*[150] mice without describing any bone abnormalities. Interestingly, DKO of *Sfrp1*/*Sfrp2* results in embryonic lethality,[151] whereas *Sfrp2*/*Sfrp5* DKO mice are viable.[150] Lexicon did not detect any skeletal phenotypes in *Sfrp2* or *Sfrp5* KO mice. *Sfrp2* KO mice have subtle limb deformities including brachydactyly and syndactyly[152] and these digit abnormalities were likely missed in Lexicon's HTS.

Published reports describe skeletal phenotypes in *Sfrp1* and *Sfrp3* KO mice. Global overexpression of *Sfrp1* in transgenic mice results in reduced bone mass.[153] *Sfrp1* KO mice have elevated trabecular bone mass after 13 weeks of age,[154–155] but Lexicon's primary and secondary screens did not confirm this observation. Interestingly, the published *Sfrp1* KO (targeting exon 1) mice examined were generated at Lexicon prior to 2000. These mice are distinct from the KO mouse subsequently studied at Lexicon. The reason for this discrepancy is unclear and additional studies are required. DEXA HTS analyses performed at the Harwell MRC site as part of the Europhenome mouse KO project observed reduced BMD in *Sfrp1* KO mice. At least three additional *Sfrp1* KO mice lines have been generated[151,156–157] without skeletal analyses performed.

Frzb (Sfrp3) KO mice have normal trabecular bone mass but a 7% increase in cortical bone thickness and increased articular cartilage loss during arthritis triggered by instability, enzymatic injury or inflammation.[158] KO mice also showed an exaggerated cortical bone gain in response to repetitive loading of the ulna, with the added bone being predominantly periosteal.[157] Loss of bone following ovariectomy was not affected by *Sfrp3* KO.[157] GWAS analysis identified *SFRP3* SNPs that influence hip osteoarthritis and geometry.[159] Lexicon's HTS and secondary screens did not show an obvious bone phenotype. Further analysis of the secondary screen microCT data (excluding one KO outlier) found a 6% increase in midshaft femur cortical thickness ($P=0.07$, with $N=8$ for both WT and KO mice). No challenge studies, such as mechanical loading, were performed.

Including Lexicon's data, three independent laboratories have presented data in abstracts showing bones from *Sfrp4* KO mice have increased trabecular bone mass, elevated cortical bone diameter and reduced cortical bone thickness.[30,160–161] High trabecular bone mass results in increased compressive breaking strength of the LV5 vertebral body, whereas reduced cortical bone thickness leads to reduced four-point breaking strength of the femur shaft.[30] Differential effects of disrupting *Sfrp4* function in cortical and trabecular bone likely reflect distinct signaling pathways as canonical WNT signaling is involved in trabecular bone formation but non-canonical Wnt signaling is involved in cortical bone formation.[162] The Yale/Harvard and Lexicon data are being prepared for a joint publication. Here we show our HTS and secondary screen data characterizing these skeletal phenotypes and data from a *Sfrp4*/*Wnt16* DKO study.

As described above, *Wnt16* KO mice have normal trabecular bone mass but reduced cortical bone diameter and thickness. We examined the effects of disruption of WNT16 signaling on the skeletal phenotypes of male and female *Sfrp4* KO mice by microCT at 16 weeks of age. In the absence of an effect of *Wnt16* KO on trabecular bone, the elevated trabecular bone mass in *Sfrp4* KO mice should not be influenced by disruption of *Wnt16*. However, the enlarged cortical bone diameter in *Sfrp4* KO mice might involve WNT16 signaling. Since cortical bone thickness is reduced in both *Sfrp4* and *Wnt16* KO mice, simultaneous disruption of both genes might result in greatly reduced thickness and even spontaneous fractures.

As shown in Supplementary Table S2, skeletal phenotypes in both male and female *Sfrp*4 and *Wnt16* single KO mice are exactly as determined previously. LV5 trabecular bone is elevated in *Sfrp4* KO mice but normal in *Wnt16* KO mice. Cortical bone total area (diameter) is elevated in *Sfrp4* KO mice and reduced in *Wnt16* KO mice. Cortical thickness is reduced in both KOs, but to a greater extent with *Sfrp4* than *Wnt16* disruption. KO of *Wnt16* did not influence the elevated LV5 trabecular bone mass in *Sfrp4* KO mice. Bones from DKO mice had intermediate cortical total area between elevated *Sfrp4* KO and reduced *Wnt16* KO values (interaction P values >0.50), indicating these two genes have independent actions on bone diameter. Bone areas were reduced similarly in both KOs and not further influenced by DKO. Marrow areas were greatly elevated with KO of *Sfrp4*, slightly reduced with KO of *Wnt16* and elevated in DKOs.

Table 4. Primary and secondary screen data for KOs with robust bone phenotypes

Gene	Analysis	*N*	vBMD/%	Spine BMD/%	Femur BMD/%	LV5 TBV/%	Femur CT/μm
Control Data	HTS	—	100	100	100	16	246
Dcstamp	HTS	12	96	102	96	20	247
	SS	24	100	98	98	26	284
Gnptab	HTS	12	93	90	92	9	210
	SS	14	99	87	101	13	275
Kiss1	HTS	12	91	89	90	8	208
	SS	25	93	79	92	12	252
Kiss1r	HTS	12	90	75	81	10	203
	SS	19	77	73	82	12	213
Mstn	HTS	12	97	109	101	17	227
Slc30a5	HTS	12	91	89	85	4	206
	SS	52	93	98	93	7	235

Mouse ages in the secondary screens were 30 weeks for *Dcstamp*, 16 weeks for *Gnptab*, 27 weeks for *Kiss1*, 15 weeks for *Kiss1r*, and 24 weeks for *Slc30a5*. HTS=high-throughput primary screen; SS=secondary screen.

Therefore, inactivation of *Wnt16* does not prevent the stimulation of endocortical bone resorption responsible for the enlarged marrow cavity in *Sfrp4* KO mice. Bones from DKO mice had lower cortical thickness than the already reduced values in single KOs but no spontaneous fractures were observed.

Like SFRPs, WNT inhibitory factor 1 antagonizes Wnt signaling by binding to WNTs. *Wif1* KO mice have a normal skeleton but are sensitive to radiation-induced osteosarcomas[163] and mice with osteoblast-specific *Wif1* overexpression display no overt bone phenotype.[164] Lexicon's *Wif1* KO mice had no clear bone phenotypes in HTS or secondary screens.

WNT10A suppresses adipogenesis and stimulates osteoblastogenesis in ST2 and 3T3-L1 cells.[165] Lexicon's HTS did not identify a bone phenotype in *Wnt10a* KO mice, but follow-up studies showed a 5% decrease in body length in both male and female KO mice at 33 weeks of age (data not shown). WNT10B is expressed in primary cultures of mature mouse calvarial osteoblasts[166] and activates canonical WNT signaling in the immune system, mammary gland, adipose tissue, bone and skin.[167] *Wnt10b* KO mice develop low bone mass with age.[168] Transgenic mice with high *Wnt10b* expression driven by the FABP4 promoter in adipocytes and the osteocalcin promoter in osteoblasts have HBM.[169–170] The anabolic effect of teriparatide treatment involves WNT10B stimulation of T lymphocytes.[171] Lexicon's *Wnt10b* KO mice showed modestly low bone mass in the HTS and follow-up studies. At 32 weeks of age (Supplementary Table S3), vBMD was reduced 8% in both male and female mice. MicroCT analyses indicated reduced LV5 trabecular number but normal cortical bone total area (diameter) with minimal decreases in cortical thickness.[28]

KOs with robust bone phenotypes

Table 4 provides HTS and secondary screen data for seven KOs having clear bone phenotypes.

The seven-pass transmembrane protein DCSTAMP is required for fusion of mouse osteoclast precursors,[172–174] and this observation was confirmed in Lexicon's *Dcstamp* KO mice. All osteoclasts are mononuclear, indicating a complete block in osteoclast cell fusion. There appeared to be increased numbers of mononuclear osteoclasts and bone architecture appeared normal by histology (Supplementary Figure S1i). Surprisingly, bone mass was only minimally elevated in the original work and normal in Lexicon's HTS and secondary screens.

GNPTAB codes for the alpha and beta subunits of the GlcNAc-1-phosphodiester α-*N*-acetylglucosaminase, which is synthesized as a type III membrane precursor protein subsequently activated by site-1 protease. Patients with mutations in *GNPTAB* suffer from mucolipidosis type II which involves missorting of lysosomal proteins. Among other phenotypes, these patients have disabling skeletal abnormalities. Transgenic mice with a single base-pair insertion into *Gnptab* mimicking a human mutation are osteopenic from reduced bone formation and enhanced osteoclast activity.[175] Lexicon's HTS and secondary screen showed KO mice have reduced bone mass in the spine. Lexicon has published a full analysis of the retinal defects in these KO mice, with data on body weight and length and cartilage histologic abnormalities.[176] *Gnptg* KO mice with disruption of the gamma subunit of this enzyme have only minor defects, presumably due to residual beta-glucuronidase activity.[177]

KISS1R (kisspeptin1 receptor, GPR54) is a hypothalamic G-coupled receptor activated by the peptide Kisspeptin to initiate gonadotropin releasing hormone secretion at puberty. Mutations in either this ligand or its receptor result in hypothalamic hypogonadism in both sexes and KO mice continue to provide valuable insights into reproductive physiology.[178–179] Lifelong KO of *Kiss1* or *Kiss1r* in mice should produce similar phenotypes to those observed with orchidectomy or ovariectomy prior to puberty. As expected, histological examinations showed Lexicon's

Kiss1 and *Kiss1r* KO mice both had typical lesions of hypogonadotropic hypogonadism including immature gonads and absence of sexual dimorphism (kidney and salivary glands in the male, mammary gland in the female). All bone parameters were low in the HTS and secondary screens. For *Kiss1r* KOs, DEXA and microCT data from the secondary screen are provided in Supplementary Figure S2. Both male and female KO mice were obese, but through different mechanisms. Male mice had normal body fat content but low LBM, whereas female mice had normal LBM but excess body fat.[180]

Myostatin is a secreted protein that inhibits myogenesis with spontaneous mutations in humans, dogs and cattle resulting in dramatic muscle hypertrophy. In addition to muscle hyperplasia, *Mstn* KO mice have elevated bone mass.[181–183] In Lexicon's HTS, *Mstn* KO mice had high muscle mass as determined by DEXA LBM (129% of normal), QMR LBM (126% of normal), gastrocnemius muscle weight (198% of normal) and increased muscle fiber number but not size by histology. An additional seven KO and five WT male mice were examined at 116 weeks of age (Supplementary Table S4). As expected, QMR LBM (120%) and gastrocnemius weight (188%) were increased. Spine trabecular bone, femur and tibia lengths (data not shown) and cortical bone diameters at the femoral midshaft or tibia–fibula junction were all unaltered in KO mice. Cortical bone thickness was elevated at the femoral midshaft and tibia–fibula junction. Cortical bone in the distal tibia (halfway between the tibia–fibula junction and the distal bone end) had an enlarged diameter but normal thickness. These site-specific bone changes demonstrate that distinct skeletal locations are influenced by lifelong muscle hypertrophy.

SLC30A5 is a zinc transporter with *Slc30a5* KO mice reported to have extremely low bone mass[184] and this observation was confirmed for Lexicon's KO mice in both primary and secondary screens. Mechanisms responsible for this severe osteopenia are unclear.

KOs with minor bone phenotypes

Table 5 provides HTS and secondary screen data for ten KOs having minor bone phenotypes.

KO of the calcitonin receptor (Calcr) in mice led to embryonic lethality when exons 6 and 7 were targeted[185] but normal viability and trabecular bone mass in spine and femur when exons 13 and 14 were targeted.[186] Lexicon's *Calcr* KO mice were generated by targeting exon 1 and no clear bone phenotype was observed in the HTS.

Gremlins are BMP inhibitors and osteoblast-specific KO of *Grem1* results in transiently elevated trabecular bone mass.[187] Global *Grem1* KO mice, examined in a C57BL/6-FVB hybrid background to minimize neonatal lethality occurring in C57BL/6 mice, had reduced growth rates, missing fibula and generally low trabecular bone mass.[188] Human GWAS studies identified *GREM2* SNPs that influence hip bone mass[189] and trabecular but not cortical bone.[190] Craniofacial development in zebrafish is influenced by GREM2 expression, as part of a regulatory system involving BMP4, endothelin-1 and jagged 1b.[191] Lexicon's *Grem2* KO mice showed elevated spine and femur BMD in the HTS and dental defects.[192] Additional studies are required to characterize possible skeletal phenotypes in this mouse KO.

IL6RA codes for the IL-6 receptor-alpha and an antibody to this receptor (tocilizumab) is an effective treatment for rheumatoid arthritis. In studies of *Il6ra* KO mice, no skeletal phenotypes were observed but one of two studies[193–194] indicated that KO mice are protected from ovariectomy-induced bone loss. Treating normal mice with an IL-6 neutralizing antibody following ovariectomy has given conflicting results, both inhibiting bone loss[195] and being without effect.[196] Secondary hyperparathyroidism from dietary calcium deficiency produced similar bone loss in WT and IL-6 KO mice.[197] Transgenic mice overexpressing IL-6 are growth retarded and have low bone mass.[198] Continuous low-dose PTH infusion in normal mice increases levels of serum IL-6 and bone resorption markers. This

Table 5. Primary and secondary screen data for KOs with minor bone phenotypes

Gene	Analysis	*N*	vBMD/%	Spine BMD/%	Femur BMD/%	LV5 TBV/%	Femur CT/μm
Control Data	HTS	—	100	100	100	16	246
Calcr	HTS	12	100	93	98	16	245
Grem2	HTS	12	101	113	110	9	221
Il6ra	HTS	12	101	NM	NM	15	264
Slc26a7	HTS	12	101	107	103	30	253
Slc39a1	HTS	12	100	96	105	22	290
Sparc	HTS	12	98	89	95	9	243
	SS	44	98	96	97	14	261
Spp1	HTS	12	103	97	102	17	260
Ssh1	HTS	12	110	120	117	10	221
Sostdc1	HTS	12	102	99	100	16	252
Wnt5b	HTS	13	107	109	110	20	258
	SS	24	113	110	112	20	269

Mouse ages in the secondary screens were 26 weeks for *Sparc* and 19 weeks for *Wnt5b*. HTS=high-throughput primary screen; SS=secondary screen.

PTH-stimulated bone resorption, but not bone formation, was suppressed with cotreatment with an IL-6 neutralizing antibody.[199]

FACS analysis confirmed that isolated spleen cells from Lexicon's *Il6ra* KO mice ($N=10$ for both KO and WT) did not bind a commercial IL-6 receptor antibody. KO mice had normal bone mass in Lexicon's HTS and normal body, spine and femur BMD in two additional cohorts (21 and 25 weeks of age (Supplementary Table S5A). Mice in both cohorts underwent sham or ovariectomy surgery with bone analyses on the combined cohorts after 6 weeks. There was no effect of *Il6ra* KO on bone loss following ovariectomy, determined by both DEXA BMD scans and microCT analyses of spine BV/TV and midshaft femur diameter and cortical thickness (Supplementary Table S5B). Treating a third mouse cohort (97 weeks of age) with teriparatide produced similar elevations in serum PINP levels in control and KO mice (Supplementary Figure S3a), suggesting IL-6 is not involved in the anabolic actions of teriparatide.

SLC26A7 is an anion transporter with *Slc26a7* KO mice having reduced gastric acid secretion and distal renal tubular acidosis.[200] Lexicon's *Slc26a7* KO mice were hypothyroid with males more strongly affected than females. Serum thyroxine levels ($N=6$ or 7) were reduced by 87% in males ($P<0.001$) and 47% in females ($P=0.003$). Histologic observations showed hyperplastic thyrotrophs in male but not female mice. Bone mass was slightly elevated in the HTS screen. Follow-up studies examined male and female mice separately between 18 and 21 weeks of age (Supplementary Table S6). Consistent with modest hypothyroidism, there were minimal effects of *Slc26a7* KO on bones from female mice. Male mice, being severely hypothyroid, had modest reductions in LBM (20%) and femur length (6%), but elevated vertebral trabecular bone as indicated by high spine BMD (20%), LV5 trabecular BV/TV (42%) and LV5 trabecular thickness (28%).

The sodium/iodide symporter SLC5A5 plays a major role in thyroid iodide uptake and mutations in this gene result in hypothyroidism. Analyses of 12 different *SLC5A5* mutations shows marked clinical heterogeneity in patients with the same and different mutations without a clear genotype-phenotype correlation. This observation '… suggests that additional unknown factors are involved in the clinical manifestation' of this defective iodide transport.[201] There do not appear to be any data for *Slc5a5* KO mice. SLC26A4 (PENDRIN) is an anion exchanger with broad specificity, including iodide, and *Slc26a4* KO mice are deaf without a thyroid phenotype.[202] Since *Slc26a7* KO mice are hypothyroid, this anion transporter might also contribute to iodide uptake by thyrotrophs as mouse SLC26A7 is capable of both chloride and iodide transport.[203]

SLC39A1 is a zinc transporter expressed in osteoclasts.[204] Triple KO of mouse *Slc39a1*, *Slc39a2* and *Slc39a3* did not produce an obvious phenotype unless the mice were fed a zinc-deficient diet.[205] Lexicon's *Slc39a1* KO mice had normal BMD and LV5 trabecular bone in the HTS but elevated cortical thickness. MicroCT analyses of bones from a second cohort of female mice examined at 42 weeks of age ($N=18$ for WTs and $N=21$ for KOs) confirmed the lack of a LV5 trabecular bone phenotype and femur length was normal. Midshaft cortical bone scans at 6 micrometer voxel size showed elevated total area (23%, $P<0.001$) and cortical thickness (6%, $P=0.09$) but reduced material BMD (3.2%, $P<0.001$) consistent with cortical porosity visually observed in the scans.

SPARC (secreted protein, acid, cysteine-rich, also known as osteonectin) is a widely expressed matricellular glycoprotein that has been extensively studied. Two of three Lexicon *Sparc* KO mice examined had cataracts, as previously reported.[206–207] KO mice have increased subcutaneous fat with normal body weight.[208] Lexicon's KO mice did not have an obesity phenotype when fed mouse chow or high fat diet (data not shown) but subcutaneous fat was not examined. KO mice develop intervertebral disk degeneration with aging,[209] but this defect was not noticed in Lexicon's mature KO mice. Several studies have reported modest osteopenia in KO mice[210–212] and Lexicon's *Sparc* KO mice showed trends for low bone mass.

Secreted phosphoprotein 1 (osteopontin) is a widely-expressed, highly acidic SIBLING phosphoprotein degraded into small fragments by PHEX[213] and having many non-skeletal actions. Numerous abnormalities, including fibrosis, abnormal wound healing, defective cardiac remodeling, tumor metastases, aberrant angiogenesis and ectopic calcification, have been observed in *Spp1* KO mice. Trabecular bone mass has been reported to be both normal[214–216] and high.[217–220] Lexicon's *Spp1* KO mice had normal bone mass in the HTS.

Actin plays a critical role in osteoclast activity and is a component of the podosome and ruffled borders. Actin dynamics are regulated by many factors[221] including cofilin, one of the most highly expressed genes in osteoclasts.[222] There are three cofilin genes: cofilin1, cofilin2 and destrin (actin depolymerizing factor). Lexicon's KOs of *Cfl1* and *Cfl2* were both embryonic lethal, with no bone phenotypes in HTS or secondary screens for heterozygous mutant mice. KO of destrin increases bone loss following unloading.[223] Cofilin activity is inhibited by LIM kinase phosphorylation and reactivated after dephosphorylation by slingshot phosphatases.[224–226] Osteoclasts isolated from *Limk1* KO mice are hyperactive and published *Limk1* KO mice have spine abnormalities[227] and reduced bone mass.[228] However, Lexicon's *Limk1* and *Limk2* KO mice

had no HTS skeletal phenotypes. There are three members in the Slingshot (SSH) family and disruption of Slingshot activity might suppress osteoclast activity. KOs of *Ssh2* and *Ssh3* did not have HTS skeletal phenotypes (data not shown), but *Ssh1* KO mice had HBM in the HTS and three additional cohorts of KO mice were examined (data not shown). Elevated bone mass was confirmed in Cohort #1 female, but not male mice; was not confirmed in Cohort #2 female mice (males were not examined); and was confirmed in Cohort #3 male and female mice. *Ssh1* KO did not protect Cohort #3 mice from ovariectomy-induced bone loss between 16 and 24 weeks of age. Given its small magnitude, the inconsistency of this skeletal phenotype is not surprising. Normal bone loss following ovariectomy made this gene uninteresting as an osteoporosis drug target. *Ssh2* and/or *Ssh3* might also be active in osteoclasts and a double or triple KO study is required to examine this topic.

Sclerostin domain containing 1 (*SOSTDC1*) codes for Wise (Ectodin) protein, which has a close homology to sclerostin and also inhibits canonical Wnt signaling by binding to Lrp5 and Lrp6. Lexicon's *Sostdc1* KO mice did not show any obvious skeletal phenotypes in the HTS, consistent with observations of no phenotype[229] and mildly elevated BMD through 3 months of age that disappears at 4 months of age.[230]

Robinow syndrome, with major skeletal abnormities, results from mutations in *WNT5A*.[231] KO of *Wnt5a* results in perinatal lethality[232] with mouse fetuses having numerous dental[233] and skeletal[234] defects. *Wnt5a* heterozygous mutant mice exhibit impaired osteoclastogenesis.[235] Skeletal actions of *Wnt5b* are less clear, as KO mice have been examined only for neuronal development.[236] Chondrocyte hypertrophy and bone mineralization are delayed in transgenic mice overexpressing *Wnt5b* in cartilage.[234] Lexicon's *Wnt5b* KO mice had elevated bone mass in the HTS and secondary screens. Studies on additional cohorts of male and female mice showed *Wnt5a* KO mice often had slightly elevated bone mass, but this phenotype was not consistently observed (data not shown). The low magnitude of this potential elevated bone mass phenotype does not permit definitive conclusions about *Wnt5b*.

Novel genes with detrimental bone phenotypes

SLC10A7 is a Na cotransporter with unknown substrate specificity. Lexicon's *Slc10a7* KO mice exhibited moderate skeletal dysplasia (osteochondrodyplasia), characterized by markedly shortened and mildly bowed limbs. In contrast to the shorted diaphyseal regions of the bone, the epiphyses and joints were of normal size and the proximal metaphyses were mildly flared, suggesting that limb shortening was due to reduced endochondral bone growth (data not shown). At necropsy, the knees and other joints were loose due to ligamentous laxity, which would contribute to bowing of the legs during development. KO mice were small, as LBM was 77% of normal. The HTS indicated reduced bone mass (88% for spine BMD and 90% for femur BMD). MicroCT scans gave normal values for LV5 BV/TV (16%) and midshaft femur (269 μm for CT and 1.8 mm^2 for total area).

SLC25A1 is a mitochondrial citrate transporter. Lexicon's *Slc25a1* KO mice were small and sickly and surviving mice were examined at 2 weeks of age. Microscopic analysis revealed generalized hypoplasia. At the growth plate, the zones of hypertrophy were narrowed and there were notable reductions in the number of osteoblasts and the amount of osteoid. These lesions are suggestive of a metabolic deficit, resulting in a generalized hypoplasia that was most severe in liver, bone and bone marrow (data not shown).

SLC30A10 is a manganese transporter and patients with gene mutations have hypermanganesemia and Parkinsonian-like gate disturbances.[237] Lexicon's *Slc30a*10 KO mice were sickly and euthanized at 8 weeks of age. There were multiple abnormalities, including osteopenia, characterized by the loss of most trabecular bone at the metaphyses (data not shown).

Miscellaneous genes/topics

For most genes, the KO strategies employed completely inactivate gene function and genetically null mice are examined. Occasionally translation of some exons results in expressed proteins having residual activities, providing information on functions of various protein domains and their tissue specificity. This topic was mentioned above for *Lrrk1*, as Lexicon's KO mouse is osteopetrotic whereas a different KO targeting strategy results in neonatal lethality. Two additional examples (*Clnc7*, *Hdac4*) from Lexicon's database should be mentioned.

Mutations in the *CLCN7* chloride channel gene produce osteopetrosis in human patients and several groups have observed osteopetrosis in *Clcn7* KO mice. Transgenic mice having their *Clcn7* gene engineered to contain the human CLCN7 G213R missense mutation develop lethal osteopetrosis.[238] Although *Clcn7* KO mice generated at Lexicon showed retinal and neuronal degeneration, their skeletons and coat color were normal. All *Clcn7* KOs show growth retardation with poor viability and Lexicon's mice were examined at 6 weeks of age. Lexicon's KO mice were generated by disruption of exon 1, allowing expression of an active bone-specific *Clcn7* isoform that did not involve translation of the first exon.[239] Previous studies involved disruption of exons 3–7[240–241] or 8–10.[241]

The histone deacetylase 4 gene contains 31 exons, with the N-terminal portion of the protein interacting with

MEF2C and RUNX2 and the C-terminal portion containing the deacetylase domain. *Hdac4* KO mice generated by targeting exon 6 do not survive to weaning and have chondrocyte hypertrophy similar to that observed with KO of *Runx*2.[242] This lethality and chondrocyte defect can be rescued in the presence of *Mef2c* heterozygosity.[243] Lexicon examined *Hdac4* KO mice generated by gene trapping with an insertion between exons 15 and 16, allowing (reduced) expression of the MEF2C and RUNX2 interacting domains but disrupting the C-terminal deacetylase domain.[244] These *Hdac4* KO mice survived for at least 12 months without any obvious skeletal abnormalities and minimal neurological defects. HTS DEXA scans gave 101% for vBMD, 101% for spine BMD and 96% for femur BMD. MicroCT scans gave normal values for LV5 BV/TV (17%) and midshaft femur (222 μm for CT and 2.68 mm^2 for total area). LBM was slightly low, at 89% in the HTS and 86% in high fat diet challenged mice.

Mutations in *PLEKHM1* in both human and the spontaneous *incisors absent* rat cause severe osteopetrosis.[245–246] In contrast, Lexicon's *Plekhm1* mouse mutation had normal bone mass in the HTS with no evidence of osteopetrosis. This allele was generated through gene-trapping and carries an insertion within the first intron of the gene. RT-PCR of RNA collected from heart and kidney tissue clearly demonstrated the lack of endogenous transcription in the homozygous mutant animals (Supplementary Figure S3b). This lack of bone phenotype was independently confirmed in 8-week-old male mice, with lack of PLEKHM1 protein expression verified by western blotting of osteoclasts generated from KO mice (Fraser Coxon, University of Aberdeen; personal communication). The reason for this phenotype difference between mice and humans/rats with gene disruption is unclear.

Since Lexicon is primarily interested in identifying genes affecting bone mass for evaluation as osteoporosis drug targets, KO mice were not specifically examined for craniofacial abnormalities. However, histological examinations detected several KOs with abnormal craniofacial structures. We previously described hydrocephalus with craniofacial abnormalities in *Stk36* (serine threonine kinase 36) KO mice as part of an analysis of 12 KO lines having hydrocephalus.[247] Lexicon's KO of *Usp34* (ubiquitin-specific peptidase 34) resulted in half of the mice dying prior to 4 weeks of age. Surviving mice grew poorly and exhibited numerous neurologic abnormalities with lymphoid and hepatocyte hypoplasia. Flattened skulls were noted during behavior testing, but no additional observations were made. There does not appear to be any published mouse KO for this gene.

Disruption of the *Pgap1* (post-GPI attachment to proteins 1) gene by KO[248] and ENU-generated mutation[249] results in severe developmental facial abnormalities with incomplete penetrance in KOs and strain dependence with ENU mutations. Two Lexicon *Pgap1* KO mice were born with no facial features (Supplementary Figure S1j), lacking nostrils, mouth, tongue, mandible and ear canals. Eyes and other structures of the face were hypoplastic and deformed. However, most KOs survived into adulthood with reduced BW and length. For survivors, DEXA scans gave 85% for LBM, 97% for vBMD, 82% for spine BMD and 87% for femur BMD.

RASSF5 is a tumor suppressor gene and the published mouse KO study focused on oncologic parameters.[250] Lexicon's *Rassf5* KO mice had craniofacial malformations noted by gross observations and CAT scans (skulls had reduced length, a short nasal bone, a short zygomatic bone and a short mandible with a stunted coronoid process). There was histological evidence of sternal malformation consistent with chondrodysplasia (Supplementary Figure S1k). Post-cranial skeletal architecture appeared generally normal at 102% for vBMD and 99% for femur BMD. Trabecular bone mass might be elevated as spine BMD was 110% of normal and LV5 trabecular BV/TV (23%) was slightly elevated.

The three steps in ascorbic acid synthesis starting from *D*-glucuronate are catalyzed by aldehyde reductase/aldose reductase, gulonolactase, and gulonolactone oxidase. The genes coding for these four enzymes are *AKR1A1*, *AKR1B3*, *RGN* and *GULO*, respectively. *Rgn*[251] and *Gulo*[252] KO mice develop lethal scurvy and spontaneous fractures occur in *Rgn* KO mice. Haplorhini primates, guinea pigs, Shionogi (ODS) rats[253] and spontaneous fracture (Sfx) mice[254–255] all have spontaneous *GULO* gene mutations. KO of *Akr1a1* was performed at Lexicon, but these KO mice were not examined in Lexicon's HTS. *Akr1a1* KO mice develop normally but have spontaneous bone fractures during pregnancy and following ovariectomy. Further analyses showed ascorbate levels in these KO mice were 15% of normal, which are sufficient for normal development but result in scurvy during states involving oxidative stress. DKO of *Akr1a1* and *Akr1b3* results in complete ascorbic acid deficiency and scurvy.[256] Surprisingly, the contributions of aldehyde and aldose reductases to ascorbic acid synthesis were not known prior to this study.

Many genes affecting bone are also involved in tooth development.[257–258] As summarized in Supplementary Table S7, KO of *Cebpb*, *Fam20a*,[42] *Fam20c*,[42] *Grem2*,[192] *Ostm1*,[259] *Postn*,[260] *Sostdc1*[261–262] and *Src*[263] resulted in dental abnormalities.

KOs not confirming published bone phenotypes

Tryptophan hydroxylase (TPH) is the rate-limiting enzyme in serotonin synthesis and different genes code for peripheral (*TPH1*) and neuronal (*TPH2*, with two splice variants) enzymes. Greater than 90% of peripheral serotonin is

produced by gut enterochromaffin cells and acts to modulate gut motility. 5-hydroxyindoleacetic acid (5-HIAA) is a metabolic breakdown product of serotonin that cross the blood-brain barrier and urinary 5-HIAA levels can be used to estimate body serotonin turnover. 5-HIAA is also produced in the gut from the metabolism of foods, such as bananas, that contain high levels of serotonin and therefore subjects must consume restrictive diets if urinary 5-HIAA is to provide useful information.

Mouse KOs of both *Tph1* and *Tph2* are viable without gross phenotypes.[70,264–266] Lexicon examined one *Tph2* KO mouse line[264] and two distinct KOs of *Tph1*[264,266]. Brain and gut serotonin contents of *Tph2* and *Tph1* KO mice, respectively, are extremely low.

From studies on *Tph1* and *Tph2* KO mice, considerable attention has focused on potential skeletal actions of both neuronal and gut-derived systemic serotonin. Briefly, there are reports that *Tph1* KO mice with negligible circulating serotonin levels have HBM resulting from elevated bone formation,[71] whereas *Tph2* KO mice with negligible brain serotonin content have low bone mass.[267] DKOs with disruptions of both *Tph1* and *Tph2* have low bone mass.[267] These results suggest that an orally active inhibitor of gut TPH1 that does not cross the blood–brain barrier might be a novel anabolic agent for treating osteoporosis. Lexicon explored this proposed gut-derived serotonin bone anabolic response as its orally active TPH1 inhibitors are undergoing clinical trials for irritable bowel and carcinoid syndromes.[268–271]

Lexicon's *Tph1* and *Tph2* KO mice had no skeletal phenotypes in HTS analyses (Table 6). Given the therapeutic importance of TPH1 as potential drug target, additional cohorts of *Tph1* and *Tph2* KO mice were examined. These studies do not support proposals that gut-derived serotonin inhibits bone formation and brain serotonin is required for proper bone development. Bone data for Lexicon's *Tph1* KO mice (males at 4 and 7 months plus females at 7 months), along with independent data obtained in multiple cohorts of male and female KO mice from 3 through 6 months of age, have been presented.[70] Lexicon has subsequently analyzed additional *Tph1* KO mice, *Tph2* KO mice[272] and *Tph1*/*Tph2* DKO mice and detailed analyses of these studies will be reported separately.

Genes of interest with embryonic/neonatal lethality

KO of several genes having important roles in bone metabolism results in lethality of homozygous embryos. Data for heterozygous mutant *Dkk1* mice are described above. Our HTS screens evaluated heterozygous mutant mice for *Fam20b*, osteogenesis imperfecta gene *Tmem38b*, WNT coreceptors *Lrp4* and *Lrp6*, *Lrp5*/*Lrp6* chaperone *Mesdc2*, WNT secretion chaperone *Wntless* (*Gpr177*), WNT signaling regulator R-spondin2 (*Rspo2*), R-spondin receptors *Lgr4* (*Gpr48*) and *Lgr5* (*Gpr49*), glucocorticoid receptor *Nr3c1*, fibroblast growth factor receptors *Fgfr1* and *Fgfrl1*, exostosis gene *Ext1*, Wiskott–Aldrich syndrome protein *Wasf1* and its homolog *Wasf2* involved in actin dynamics, and the bisphosphonate drug target *Fdps*. In each case, there were no dramatic bone phenotypes in heterozygous mice.

SLC4A22 is a chloride-bicarbonate anion exchanger and two groups have shown *Slc4a2* KO mice survive to adulthood with reduced growth and severe osteopetrosis.[273] Lexicon's KO mice were small and sickly with death occurring about 3 weeks of age. The explanation for this difference in survivability may involve differences in mouse strains, as the other groups examined FVB/N and 129S6/SvEv Tac/Black Swiss hybrid mouse strains.

Mutations in the human gene and KO of the mouse gene coding for the lipid biosynthetic enzyme 1-acyl-sn-glycerol 3-phosphate O-acyltransferase 2 (*AGPAT2*) result in severe lipodystrophy and reduced viability.[274–275] Two of four mice *Agpat2* KO mice examined histologically at ten days of age had spontaneous proximal femur (hip) fractures.[276] No HTS bone phenotypes were observed in heterozygous mutant mice.

Sulfatase modifying factor 1 (SUMF1, formylglycine-generating enzyme) enzymatically activates all 17 sulfatases by converting a critical cysteine in the active site to formylglycine and patients with *SUMF1* mutations suffer from multiple sulfatase deficiency characterized by the combined effects of simultaneous deficiency of all sulfatases. *Sumf1* KO mice have multiple abnormalities, including reduced viability, growth retardation, seizures, kyphosis, joint deformaties and lysosomal storage disease involving GAG accumulation.[277–278] These findings were confirmed in Lexicion's KO mice, having juvenile lethality and disrupted epiphyseal cartilage maturation with absence of

Table 6. Primary screen data for *Tph1* and *Tph2* KO mice

Gene	Analysis	*N*	vBMD/%	Spine BMD/%	Femur BMD/%	LV5 TBV/%	Femur CT
Control data	HTS	—	100	100	100	16	246
Tph1 KO #1	HTS	12	99	100	103	NM	NM
Tph1 KO #2	HTS	12	99	100	101	10	221
Tph2	HTS	12	103	100	102	17	251

HTS=high-throughput primary screen; NM=not measured.

normal columnar arrays of proliferating and hypertrophic chondrocytes.

Example of a HTS false-positive bone phenotype

All HTS screens detect false-positive phenotypes and miss true phenotypes (false-negatives). False-positive hits are detected by failure to confirm the HTS phenotype in subsequent studies. One false-positive example from Lexicon's HTS is *Cytl1* (cytokine-like 1), a cytokine expressed in chondrocytes[279] that promotes chondrocyte differentiation in mouse limb bud mesenchymal cells.[280] Lexicon's *Cytl1* KO mice had a clear skeletal phenotype in the DEXA HTS, with values of 107% for body vBMD, 106% for spine BMD and 111% for femur BMD. MicroCT parameters were slightly elevated, with LV5 BV/TV being 22% and a midshaft femur cortical thickness value of 256 μm. This HTS high BMD phenotype could not be confirmed in follow-up DEXA or microCT scans of bones ($N=10$ for both male and female mice) from an additional cohort of KO mice examined at 18 weeks of age (data not shown).

DISCUSSION

This report summarizes the most comprehensive analysis to date of skeletal phenotypes observed in a HTS of gene KO mice. The number of genes examined in viable mice is many-fold higher than previous studies[1,10,24–25] and replication of phenotypes for genes previously established to affect bone mass and architecture demonstrated the effectiveness of the HTS and a low likelihood of false negatives. Identification of eight genes not previously known to have dramatic KO skeletal phenotypes suggests that many additional genes important in bone biology remain to be discovered.

Our successful HTS for identifying skeletal phenotypes in KO mice involved several key decisions.

1. Mouse phenotypes can be strongly affected by strain,[281–283] with three dramatic metabolic examples being (i) cold sensitivity in *Ucp1* KO mice;[284] (ii) obesity, diabetes and endocrine parameters in leptin-deficient ob mice;[285] and (iii) impaired insulin secretion in C57BL/6J mice.[286–287] Numerous studies have shown that bone architecture and skeletal responses to ovariectomy and exercise are influenced by the mouse strains examined. Compared to most other strains, cortical bones in C57BL/6J mice have large diameters but low thickness, and therefore low areal BMD. As shown in Supplementary Table S8, we have confirmed this common finding. As expected, midshaft femur cortical bone thickness (245 μm) in F2 hybrids is intermediate between values of the two parental strains. Values for femur length and trabecular bone in the LV5 vertebral body and distal femur metaphysis were similar for these strains. With the exception of 28 C57BL/6J KO lines (three of which were embryonic lethal), phenotyping was performed in F2 hybrids of C57BL/6J and 129 SvEv KO mice.

2. Use of DEXA allowed us to simultaneously screen both BMD and body composition (body fat and LBM). Body composition data for Lexicon's first 2322 KO lines have been published.[11]

3. Bone cell morphology was examined in decalcified histologic sections, which allowed distinction between osteopetrosis (*Src*, *Ostm1* and *Lrrk1*) and osteosclerosis (*Sost*) in KOs with HBM. The absence of multinucleated osteoclasts was detected for *Dcstamp* KO mice and bones from *Fam20c* KO mice had osteomalacia. As argued by others,[22,288–289] Lexicon's experience supports inclusion of histopathology in HTS screens of KO mice.

4. We did not include bone strength analyses in our primary HTS because biomechanical testing has high variability and we thought the possibility that bone strength would be affected independently of bone mass and architecture was low. Bone strength measurements were performed in KO lines of interest after confirmation of the skeletal phenotype. Compressive strength of LV5 is elevated with disruptions of *Sost* and *Sfrp4*,[30] whereas the strength of the femur shaft determined by three-point or four-point binding tests is greatly increased in bones from *Sost* KO mice. but decreased with *Sfrp4*[30] and *Wnt16*[38] disruption. Supplemental Figure 3c shows the excellent correlation of femur shaft strength and cortical thickness (three-point bending) in WT and *Wnt16* KO mice.[38]

5. Although we did not include bone length measurements in our primary screen, we believe this information is important in secondary screens. Bone length was unaffected in KOs of *Wnt16* and *Sfrp4* but reduced slightly with KO of *Lrrk1*.[39]

6. Analyzing global gene KOs to identify drug targets provides information on the effects of gene disruption throughout the body. Examining tissue-specific conditional KOs can address mechanistic questions related to cell types involved in biochemical pathways, but drugs act throughout the body. As a hypothetical example, consider a gene that when disrupted increases bone mass and also results in lung pathology. A drug targeting the protein coded by this gene would be expected to produce *on-target* pulmonary toxicity in addition to any beneficial skeletal effects. Examining global KOs allows drug target validation prior to starting medicinal chemistry programs.

With the experience gained performing this HTS and follow-up studies on skeletal phenotypes, several additional topics merit discussion.

1. With the exception of *Slc26a7* KO mice (with severe hypothyroidism in males but subclinical hypothyroidism in females), we did not observe clear sexual dimorphism in any of our bone phenotypes. In our opinion, gender differences in bone parameters during HTS are often spurious

statistical findings or suggestive evidence of a weak phenotype. Our experience with *Ssh1* KO mice, described above, provides a good example. High bone mass was inconsistently observed in various cohorts of KO mice, with a detectable phenotype switching between male and female mice in different cohorts. Known mutations causing established human skeletal and mineral phenotypes occur in both sexes. Both approved (bisphosphonates, teriparatide, donosumab) and experimental (cathepsin K inhibitors, sclerostin antibodies) osteoporosis therapies are effective in men and women. Mouse KO and transgenic mice show minimal skeletal sexual dimorphism with disruptions of *Lrp5, Sost, Rankl, Csk* and *Lrrk1* genes.

2. Failures by independent laboratories to confirm published preclinical findings have drawn considerable attention.[290–292] For bone research, guidelines[293] and perspectives[294] for describing skeletal phenotypes have been published. A key component of Lexicon's mouse gene KO campaign has involved comparisons to published data, with confirmations of skeletal phenotypes for 23 previously reported genes (*Calcr*, *Cebpb*, *Crtap*, *Dcstamp*, *Dkk1*, *Duoxa2*, *Enpp1*, *Fgf23*, *Kiss1/Kiss1r*, *Klotho*, *Lrp5*, *Mstn*, *Neo1*, *Npr2*, *Ostm1*, *Postn*, *Sfrp4*, *Slc30a5*, *Slc39a13*, *Sost*, *Src*, *Sumf1* and *Wnt10b*). As described above, such confirmation was not obtained for *Sfrp1*, *Tph1* and *Tph2*. Lexicon's data for *Sfrp1* are limited and further studies are clearly indicated. Lexicon negative findings for *Tph1* KO mice have been independently replicated and are consistent with additional studies performed at multiple laboratories.[70] The failure to confirm published *Clcn7* and *Hdac4* KO phenotypes is believed to result from different gene KO targeting strategies. The failure to observe osteopetrosis in *Plekhm1* KO mice, which occurs with gene disruption in rats and humans, requires further study. We strongly believe that KO comparisons to WT littermate/cagemate mice are essential to control for environmental variables and possible genetic drift of the colony.

3. Analyzing LV5 vertebral bodies and midshaft by microCT provided data on both trabecular (LV5) and cortical (femur) bone. As shown by the skeletal phenotypes observed in *Klotho*, *Src*, *Wnt16* and *Sfrp4* KO mice, these two bone compartments can have distinct responses to gene deletion. For trabecular bone examinations, we believe that LV5 is superior to the distal femur and proximal tibia, as the amount of trabecular bone present is far greater and independent of both sex and age. Performing microCT scans of the distal femur metaphyseal trabecular bone remained an option since the entire femur was obtained at necropsy. Using both DEXA and microCT scans provided both global (DEXA) and focused (MicroCT) assessments of bone mass. Having both DEXA spine BMD and microCT LV5 trabecular bone volume data provided two vertebral measurements as a check for internal consistency.

4. Strength is compromised if bone is either under- or over-mineralized. Bone mineralization is readily assessed by material BMD determined during the microCT scans. Consistent with hypophosphatemia and histologic osteomalacia, bones from *Fam20c* KO mice had reduced material BMD.[42]

5. We developed microCT methods to determine architecture of the mouse femoral neck and observed bone phenotypes at this site are consistent with the phenotypes observed at LV5 and the midshaft femur.[295] Additional experience indicates the thickness of the LV5 cortical shell responds similarly to genetic variations in midshaft femur cortical thickness. Both cortical sites lose bone following ovariectomy and gain bone with teriparatide treatment (data not shown).

6. KO mouse phenotypes can vary depending on the genetic alteration employed. If a specific protein domain is selected for disruption and the corresponding exons are deleted, other exons of the gene can still be transcribed and translated, and partial gene function may remain. Two examples described above were Lexicon's KO alleles of *Clcn7* and *Hdac4*. Another example comes from studies of the vitamin D receptor (VDR), which contains an N-terminal DNA-binding domain and a C-terminal ligand-binding domain. Nutritional vitamin D deficiency and KO of the vitamin D 1-hydroxylase (*Cyp27b1*) result in hypocalcemic rickets in mice, although mice have normal fur. Initial KO studies of *Vdr* described rachitic and hairless (alopecia) mice, whereas humans with *VDR* mutations are always rachitic but alopecia is variable. Mutations in subjects with hair occur in the ligand-binding domain, leaving the DNA-binding domain intact.[296] Thus, the VDR DNA-binding domain acts (through heterodimerization with RXR) in keratinocytes to promote hair growth without requiring binding of vitamin D. This phenotypic domain specificity also occurs in mice, as *Vdr* KO mice had rickets but normal fur if the *Vdr* ligand-binding domain was disrupted with the *Vdr* DNA-binding domain remaining intact.[297]

7. Although attention is usually focused on genes yielding phenotypes when disrupted, mutated genes that do not have bone and/or any obvious phenotypes also provide important and oftentimes surprising information.[298] For example, Lexicon's albumin (*Abl*) KO mice, having negligible levels of serum albumin, showed no obvious phenotype (data not shown). This observation is consistent with findings in analbuminemic humans and spontaneous mutant analbuminemic rats.[299] Mouse KOs of *S100g* (Calbindin9K), a Ca-binding protein,[300–302] and *Trpv6*, a putative membrane Ca transporter,[303] both failed to show expected intestinal calcium malabsorption phenotypes. Three examples of human genes acquiring loss-of-function mutations with only benign phenotypes are *MC1R* (red hair), *ABO* (O blood group) and *CCR5* (HIV resistance). Recent

explorations of the human genome have identified healthy people having genes with predicted loss-of-function homozygous mutations.[304–306] The occurrence of genes in healthy individuals having loss-of-function compound heterozygous alleles has been less thoroughly explored.

Genes can have critical functions only under environmental conditions not occurring during standard mouse phenotyping. Examples include (i) the GCN2 kinase regulating feeding behavior in response to meals with imbalances of essential amino acids;[307] (ii) KO of the mitochondrial uncoupling protein UCP1 influences body fat depending on the age of the mice and the ambient temperature at which they are housed;[308] (iii) normal iron status with KO of the iron-binding protein lactoferrin,[309] but elevated colorectal dysplasia following inflammation;[310] and (iv) *Gc* KO mice without the serum vitamin D-binding protein have normal serum bioactive vitamin D levels but respond more quickly to dietary deficiency and show hypercalcemic toxicity at lower vitamin D doses.[311–312] Compared to sedentary KO mice, physical exercise (treadmills and running wheels) can uncover pathological phenotypes in otherwise healthy KO mice (*Mybpc3*, *Lipe*) or prevent obesity in *Mc4r* KO mice.[313] Thus, KO mouse lines without skeletal phenotypes in HTS might show abnormal disturbances in bone metabolism with increasing age or following challenges such as ovariectomy, mechanical loading or unloading, fracture healing, arthritis induction, dietary deficiencies and reproduction.

8. Comparisons of skeletal phenotypes showed excellent agreement for genes having mutations or SNPs in humans and corresponding mouse KOs. Phenotype concordance was observed for *CRTAP*, *FAM20A*, *FAM20C*, *GNPTAB*, *LRP5*, *NPR2*, *OSTM1*, *SLC39A13*, *SOST* and *WNT16*, with *PLEKHM1* being the single exception.

9. During 2012, the IMPC estimated that ~30% of mouse KO lines are embryonic or perinatal lethal[314] and increasing efforts are being focused on examining embryos to determine mechanisms involved in the developmental defects.[314–315] With 556 KO lines examined, the February 2014 IMPC update lists lethal (21%) and subviable (9%) lines. Analyses of the MGI database found lethality in 23% of 6812 mouse KO genes curated[316] and 2 472 lethal gene KOs (39%) among 6283 genes annotated to have direct human orthologs.[317] A comprehensive review described birth trauma, respiratory failure, homeostasis deficiencies and inability to suckle as common causes of lethality during the first 24 h after birth.[318] KO lethality is influenced by mouse strain and can sometimes be rescued by simultaneous disruptions in different genes, as is the case of *Dkk1* KO survivability in the presence of *Wnt3* heterozygosity described above.[133–134] The lower 18% lethality value observed by Lexicon might be related to examining few genes coding for transcription factors and structural proteins and *hybrid vigor* from studying C57BL6/J–129SvEv hybrid mice. As described above, *Dkk1* heterozygous mutant mice and KO mice examined prior to 12 weeks of age due to reduced viability can show skeletal phenotypes *(Fgf23*, *Klotho*, *Nppc*, *Npr2*, *Ostm1*, *Sgpl1*, *Slc25a1*, *SLC30a10*, *Sumf1*).

Mouse resources

There are many resources providing both KO mice and phenotype data. During 2006, Francis Collins, Director of the US NIH, stated '*A graduate student shouldn't spend a year making a knockout that's already been made. It's not a good use of resources*'.[319] There are many reviews describing the evolution of the IKMC since the 2003 Banbury Organizing Conference.[320] KO mouse genes with available ES cells and/or cryopreserved sperm are compiled in the International Mouse Strain Resource, with a link from the Mouse Genomic Informatics (MGI) website and published links to centralized mouse repositories.[321] The Gene Expression Database[322] is included within the MGI resource. To facilitate tissue-specific gene KOs, most IKMC lines include the cre driver system during the gene KO targeting design and the MGI website maintains a CrePortal providing up-to-date information. Underappreciated complications of conditional cre-loxP excision include unexpected activity in off-target tissues, mosaicism and parent-of-origin effects.[323–324] Problems with the osterix-cre mouse line have been described.[325–326]

The first compendium of 263 published mouse KO phenotypes appeared in 1995.[327] The IMPC[13] coodinates phenotype data from the IKMC, with 441 KO mouse lines fully analyzed and 643 KO mouse lines under examination (September 2014). Recent results include KOs of *Lrrk1* and *Wnt16*, both having skeletal phenotypes similar to those described by Lexicon. The MGI includes phenotype data for 251 NIH-sponsored Deltagen and Lexicon KO mouse lines.

Commentaries on genome-wide KO efforts involving zebrafish,[328] nematodes[329] and yeast[330] provide interesting perspectives for mouse KO efforts. Information on rat gene KOs is compiled in the Rat Genome Database.[331]

SUMMARY

Lexicon Pharmaceuticals, during the decade preceding the initiation of the IKMC program, successfully employed *industrialized biology* to generate and phenotype over 4 650 mouse gene knockout lines. The genes examined were highly represented in the druggable genome, foreshadowing the *Illuminating the Druggable Genome* program within the NIH Common Fund (http://commonfund.nih.gov/idg/overview). Global KO strategies involved both gene trapping and homologous recombination technologies. Phenotyping screens included a battery of tests in the areas of behavior, bone, cardiology, immuno-

logy, metabolism, oncology and ophthalmology, and included serum chemistry, histopathology and a high fat diet obesity challenge. Software was written for an internal database that tracked mice undergoing breeding and moving through the phenotyping screens and allowed investigators to view all phenotyping data for all mice. Lexicon's KO mouse campaign successfully identified previously published and novel genes influencing bone mass, architecture, strength and mineralization (the *Skeletome*). Three of these novel genes (undisclosed) code for enzymes or secreted proteins that are potential osteoporosis drug targets.

Further review of the Lexicon dataset showed elevated spine bone mass phenotypes in both primary and secondary screens for *Slc37a2* (glucose-6-phosphate/phosphate antiporter) and *Slc41a2* (Mg transporter). Further studies are required to fully characterize skeletal phenotypes in these two gene KOs.

Competing interests

The authors declare no conflicts of interest.

Acknowledgements

Ramiro Ramirez-Solis, Dianne Markesich, Elizabeth Richter, Jeff Schrick and James Piggott for HTS organization; Zheng-Zheng Shi, Laurie Minze, Luis Freay and Tim Wilkins for HTS DEXA and microCT scans; Ken Platt and Katherine Holt for molecular biology supervision; Robert Read, June Wingert, Mary Thiel, Ryan Vance and others for histopathology; Dawn Bright for DKK1 antibody generation; Deon Doree for thyroxine assays; David Harris for FACS analysis; Wade Walke and William Sonnenberg for bioinformatics; Jay Mitchell and Larry Rodriquez for HTS database management.

References

1 Moore MW. High-throughput gene knockouts and phenotyping in mice. *Ernst Schering Res Found Workshop* 2005; **50**: 27–44.
2 International Mouse Knockout Consortium, Collins FS, Rossant J, Wurst W. A mouse for all reasons. *Cell* 2007; **128**: 9–13.
3 Collins FS, Finnell RH, Rossant J. Wurst W. A new partner for the International Knockout Mouse Consortium. *Cell* 2007; **129**: 235.
4 Bradley A, Anastassiadis K, Ayadi A *et al.* The mammalian gene function resource: the International Knockout Mouse Consortium. *Mamm Genome* 2012; **23**: 580–586.
5 Schofield PN, Hoehndorf R, Gkoutos GV. Mouse genetic and phenotypic resources for human genetics. *Hum Mutat* 2012; **33**: 826–836.
6 Ramirez-Solis R, Ryder E, Houghton R, White, JK, Bottomley J. Large-scale mouse knockouts and phenotypes. *Wiley Interdiscip Rev Syst Biol Med* 2012; **4**: 547–563.
7 Friddle CJ, Abuin A, Ramirez-Solis R *et al.* High-throughput mouse knockouts provide a functional analysis of the genome. *Cold Spring Harb Symp Quant Biol* 2003; **68**: 311–315.
8 Hansen GM, Markesich DC, Burnett MB *et al.* Large-scale gene trapping in C57BL/6N mouse embryonic stem cells. *Genome Res* 2008; **18**: 1670–1679.
9 Clark HF, Gurney AL, Abaya E *et al.* The secreted protein discovery initiative (SPDI), a large-scale effort to identify novel human secreted and transmembrane proteins: a bioinformatics assessment. *Genome Res* 2003; **13**: 2265–2270.
10 Tang T, Li L, Tang J *et al.* A mouse knockout library for secreted and transmembrane proteins. *Nat Biotechnol* 2010; **28**: 749–775.
11 Brommage R, Desai U, Revelli JP *et al.* High-throughput screening of mouse knockout lines identifies true lean and obese phenotypes. *Obesity (Silver Spring)* 2008; **16**: 2362–2367.
12 Brown SD, Moore MW. The International Mouse Phenotyping Consortium: past and future perspectives on mouse phenotyping. *Mammalian Genome* 2012; **23**: 632–640.
13 Koscielny G, Yaikhom G, Iyer V *et al.* The International Mouse Phenotyping Consortium Web Portal, a unified point of access for knockout mice and related phenotyping data. *Nucleic Acids Res* 2014; **42**: D802–D809.
14 Ayadi A, Birling MC, Bottomley J *et al.* Mouse large-scale phenotyping initiatives: overview of the European Mouse Disease Clinic (EUMODIC) and of the Wellcome Trust Sanger Institute Mouse Genetics Project. *Mamm Genome* 2012; **23**: 600–610.
15 Beckers J, Wurst W, de Angelis MH. Towards better mouse models: enhanced genotypes, systemic phenotyping and envirotype modelling. *Nat Rev Genet* 2009; **10**: 371–380.
16 Brown MJ, Murray KA. Phenotyping of genetically engineered mice: humane, ethical, environmental, and husbandry issues. *ILAR J* 2006; **47**: 118–123.
17 Fuchs H, Lisse T, Hans W *et al.* Phenotypic characterization of mouse models for bone-related diseases in the German Mouse Clinic. *J Musculoskelet Neuronal Interact* 2008; **8**: 13–14.
18 Fuchs H, Gailus-Durner V, Neschen S *et al.* Innovations in phenotyping of mouse models in the German Mouse Clinic. *Mamm Genome* 2012; **23**: 611–622.
19 Justice MJ. Removing the cloak of invisibility: phenotyping the mouse. *Dis Models Mech* 2008; **1**: 109–112.
20 Murray KA. Issues to consider when phenotyping mutant mouse models. *Lab Anim (NY)* 2002; **31**: 25–29.
21 Schofield PN, Dubus P, Klein L *et al.* Pathology of the laboratory mouse: an International Workshop on Challenges for High Throughput Phenotyping. *Toxicol Pathol* 2011; **39**: 559–562.
22 Schofield PN, Vogel P, Gkoutos GV, Sundberg JP. Exploring the elephant: histopathology in high-throughput phenotyping of mutant mice. *Dis Models Mech* 2012; **5**: 19–25.
23 Zeiss CJ, Ward JM, Allore HG. Designing phenotyping studies for genetically engineered mice. *Vet Pathol* 2012; **49**: 24–31.
24 Bassett JH, Gogakos A, White JK *et al.* Rapid-throughput skeletal phenotyping of 100 knockout mice identifies 9 new genes that determine bone strength. *PLoS Genet* 2012; **8**: e1002858.
25 White JK, Gerdin AK, Karp NA *et al.* Genome-wide generation and systematic phenotyping of knockout mice reveals new roles for many genes. *Cell* 2013; **154:** 452–464.
26 Iwaniec UT, Wronski TJ, Liu J *et al.* PTH stimulates bone formation in mice deficient in Lrp5. *J Bone Miner Res* 2007; **22**: 394–402.
27 Brommage R, Liu J, Suwanichkul A, Powell DR. High bone mass in sclerostin-deficient knockout mice. *J Musculoskelet Neuronal Interact* 2006; **6**: 392.
28 Brommage R, Liu J, Revelli JP, Kirkpatrick LL, Powell DR. Gene knockouts of Wnt10b and Wnt16 in mice result in low bone mass. *Bone* 2007; **40**(Suppl 2): S187.
29 Brommage R, Liu J, Bright D *et al.* Elevated bone mass in mice treated with anti-Dickkopf-1 neutralizing antibodies. *J Bone Miner Res* 2010; **25**(Suppl 1): S81.

30 Brommage R, Liu J, Lee E. Elevated trabecular bone mass with reduced cortical bone thickness in sFRP4 knockout mice. *J Bone Miner Res* 2009; **24**(Suppl 1): S82.
31 Walke DW, Han C, Shaw J, Wann E, Zambrowicz B, Sands A. *In vivo* drug target discovery: identifying the best targets from the genome. *Curr Opin Biotechnol* 2001; **12**: 626–631.
32 Zambrowicz BP, Sands AT. Knockouts model the 100 best-selling drugs—will they model the next 100? *Nat Rev Drug Discov* 2003; **2**: 38–51.
33 Zambrowicz BP, Turner CA, Sands AT. Predicting drug efficacy: knockouts model pipeline drugs of the pharmaceutical industry. *Curr Opin Pharmacol* 2003; **3**: 563–570.
34 Russ AP, Lampel S. The druggable genome: an update. *Drug Discov Today* 2005; **10**: 1607–1610.
35 Plewczynski D, Rychlewski L. Meta-basic estimates the size of druggable human genome. *J Mol Model* 2009; **15**: 695–699.
36 Nieman BJ, Blank MC, Roman BB, Henkelman RM, Millen KJ. If the skull fits: magnetic resonance imaging and microcomputed tomography for combined analysis of brain and skull phenotypes in the mouse. *Physiol Genomics* 2012; **44**: 992–1002.
37 Medina-Gomez C, Kemp JP, Estrada K *et al.* Meta-analysis of genome-wide scans for total body BMD in children and adults reveals allelic heterogeneity and age-specific effects at the WNT16 locus. *PLoS Genet* 2012; **8**: e1002718.
38 Zheng HF, Tobias JH, Duncan E *et al.* WNT16 influences bone mineral density, cortical bone thickness, bone strength, and osteoporotic fracture risk. *PLoS Genet* 2012; **8**: e1002745.
39 Xing W, Liu J, Cheng S, Vogel P, Mohan S, Brommage R. Targeted disruption of leucine-rich repeat kinase 1 but not leucine-rich repeat kinase 2 in mice causes severe osteopetrosis. *J Bone Miner Res* 2013; **28**: 1962–1974.
40 Linares GR, Brommage R, Powell DR *et al.* Claudin 18 is a novel negative regulator of bone resorption and osteoclast differentiation. *J Bone Miner Res* 2012; **27**: 1553–1565.
41 Tagliabracci VS, Pinna LA, Dixon JE. Secreted protein kinases. *Trends Biochem Sci* 2013; **38**: 121–130.
42 Vogel P, Hansen GM, Read RW *et al.* Amelogenesis imperfecta and other biomineralization defects in Fam20a and Fam20c null mice. *Vet Pathol* 2012; **49**: 998–1017.
43 Hla T, Dannenberg AJ. Sphingolipid signaling in metabolic disorders. *Cell Metab* 2012; **16**: 420–434.
44 Lotinun S, Kiviranta R, Matsubara T *et al.* Osteoclast-specific cathepsin K deletion stimulates S1P-dependent bone formation. *J Clin Invest* 2013; **123**: 666–681.
45 Vogel P, Donoviel MS, Read R *et al.* Incomplete inhibition of sphingosine 1-phosphate lyase modulates immune system function yet prevents early lethality and non-lymphoid lesions. *PloS One* 2009; **4**: e4112.
46 Wattler S, Kelly M, Nehls M. Construction of gene targeting vectors from lambda KOS genomic libraries. *Biotechniques* 1999; 26: 1150–1156, 1158, 1160.
47 Zambrowicz BP, Holt KH, Walke W, Kirkpatrick LL, Eberhart DE. Generation of transgenic animals. In: Metcalf B, Dillon S (ed.), *Target validation in drug discovery*. New York: Elsevier Academic Press, 2006: 3–25.
48 Abuin A, Hansen GM, Zambrowicz B. Gene trap mutagenesis. *Handb Exp Pharmacol* 2007; **178**: 129–147.
49 Atasoy D, Schoch S, Ho A *et al.* Deletion of CASK in mice is lethal and impairs synaptic function. *Proc Natl Acad Sci USA* 2007; **104**: 2525–2530.
50 Gale NW, Dominguez MG, Noguera I *et al.* Haploinsufficiency of delta-like 4 ligand results in embryonic lethality due to major defects in arterial and vascular development. *Proc Natl Acad Sci USA* 2004; **101**: 15949–15954.
51 Brommage R. Validation and calibration of DEXA body composition in mice. *Am J Physiol Endocrinol Metab* 2003; **285**: E454–E459.
52 Rissanen JP, Suominen MI, Peng Z *et al.* Short-term changes in serum PINP predict long-term changes in *trabecular* bone in the rat ovariectomy model. *Calcified Tissue Int* 2008; **82**: 155–161.
53 Anderson JM, van Itallie CM. Physiology and function of the tight junction. *Cold Spring Harb Perspect Biol* 2009; **1**: a002584.
54 Wongdee K, Pandaranandaka J, Teerapornpuntakit J *et al.* Osteoblasts express claudins and tight junction-associated proteins. *Histochem Cell Biol* 2008; **130**: 79–90.
55 Doty SB. Morphological evidence of gap junctions between bone cells. *Calcif Tissue Int* 1981; **33**: 509–512.
56 Hayashi D, Tamura A, Tanaka H *et al.* Deficiency of claudin-18 causes paracellular H^+ leakage, up-regulation of interleukin-1beta, and atrophic gastritis in mice. *Gastroenterology* 2012; **142**: 292–304.
57 Alshbool FZ, Alarcon C, Wergedal J, Mohan S. A high-calcium diet failed to rescue an osteopenia phenotype in claudin-18 knockout mice. *Physiol Rep* 2014; **2**: e00200.
58 Wang X, Wang S, Li C *et al.* Inactivation of a novel FGF23 regulator, FAM20C, leads to hypophosphatemic rickets in mice. *PLoS Genet* 2012; **8**: e1002708.
59 Simpson MA, Hsu R, Keir LS *et al.* Mutations in FAM20C are associated with lethal osteosclerotic bone dysplasia (Raine syndrome), highlighting a crucial molecule in bone development. *Am J Hum Genet* 2007; **81**: 906–912.
60 Tagliabracci VS, Engel JL, Wen J *et al.* Secreted kinase phosphorylates extracellular proteins that regulate biomineralization. *Science* 2012; **336**: 1150–1153.
61 Ishikawa HO, Xu A, Ogura E, Manning G, Irvine KD. The Raine syndrome protein FAM20C is a Golgi kinase that phosphorylates bio-mineralization proteins. *PLoS One* 2012; **7**: e42988.
62 Tagliabracci VS, Engel JL, Wiley SE *et al.* Dynamic regulation of FGF23 by Fam20C phosphorylation, GalNAc-T3 glycosylation, and furin proteolysis. *Proc Natl Acad Sci USA* 2014; **111**: 5520–5525.
63 Gong Y, Slee RB, Fukai N *et al.* LDL receptor-related protein 5 (LRP5) affects bone accrual and eye development. *Cell* 2001; **107**: 513–523.
64 Kato M, Patel MS, Levasseur R *et al.* Cbfa1-independent decrease in osteoblast proliferation, osteopenia, and persistent embryonic eye vascularization in mice deficient in Lrp5, a Wnt coreceptor. *J Cell Biol* 2002; **157**: 303–314.
65 Holmen SL, Giambernardi TA, Zylstra CR *et al.* Decreased BMD and limb deformities in mice carrying mutations in both Lrp5 and Lrp6. *J Bone Miner Res* 2004; **19**: 2033–2040.
66 Li X, Ominsky MS, Niu QT *et al.* Targeted deletion of the sclerostin gene in mice results in increased bone formation and bone strength. *J Bone Miner Res* 2008; **23**: 860–869.
67 Kramer I, Loots GG, Studer A, Keller H, Kneissel M. Parathyroid hormone (PTH)-induced bone gain is blunted in SOST overexpressing and deficient mice. *J Bone Miner Res* 2010; **25**: 178–189.
68 Sawakami K, Robling AG, Ai M *et al.* The Wnt co-receptor LRP5 is essential for skeletal mechanotransduction but not for the anabolic bone response to parathyroid hormone treatment. *J Biol Chem* 2006; **281**: 23698–23711.
69 Arantes HP, Barros, ER, Kunii I, Bilezikian JP, Lazaretti-Castro M. Teriparatide increases bone mineral density in a man with osteoporosis pseudoglioma. *J Bone Miner Res* 2011; **26**: 2823–2826.
70 Cui Y, Niziolek PJ, MacDonald BT *et al.* Lrp5 functions in bone to regulate bone mass. *Nat Med* 2011; **17**: 684–691.

71 Yadav VK, Ryu JH, Suda N *et al.* Lrp5 controls bone formation by inhibiting serotonin synthesis in the duodenum. *Cell* 2008; **135**: 825–837.
72 Xu Q, Wang Y, Dabdoub A *et al.* Vascular development in the retina and inner ear: control by Norrin and Frizzled-4, a high-affinity ligand-receptor pair. *Cell* 2004; **116**: 883–895.
73 Ke J, Harikumar KG, Erice C *et al.* Structure and function of Norrin in assembly and activation of a Frizzled 4-Lrp5/6 complex. *Genes Dev* 2013; **27**: 2305–2319.
74 Lobov IB, Rao S, Carroll TJ *et al.* WNT7b mediates macrophage-induced programmed cell death in patterning of the vasculature. *Nature* 2005; **437**: 417–421.
75 Xia CH, Yablonka-Reuveni Z, Gong X. LRP5 is required for vascular development in deeper layers of the retina. *PloS One* 2010; **5**: e11676.
76 Paes KT, Wang E, Henze K *et al.* Frizzled 4 is required for retinal angiogenesis and maintenance of the blood–retina barrier. *Invest Ophthalmol Vis Sci* 2011; **52**: 6452–6461.
77 Marin I. The Parkinson disease gene LRRK2: evolutionary and structural insights. *Mol Biol Evol* 2006; **23**: 2423–2433.
78 Baptista MA, Dave KD, Sheth NP *et al.* A strategy for the generation, characterization and distribution of animal models by The Michael J. Fox Foundation for Parkinson's Research. *Dis Model Mech* 2013; **6:** 1316–1324.
79 Kim BJ, Koh JM, Lee SY *et al.* Plasma sphingosine 1-phosphate levels and the risk of vertebral fracture in postmenopausal women. *J Clin Endocrinol Metab* 2012; **97**: 3807–3814.
80 Pederson L, Ruan M, Westendorf JJ, Khosla S, Oursler MJ. Regulation of bone formation by osteoclasts involves Wnt/BMP signaling and the chemokine sphingosine-1-phosphate. *Proc Natl Acad Sci USA* 2008; **105**: 20764–20769.
81 Bagdanoff JT, Donoviel MS, Nouraldeen A *et al.* Inhibition of sphingosine-1-phosphate lyase for the treatment of autoimmune disorders. *J Med Chem* 2009; **52**: 3941–3953.
82 Bagdanoff JT, Donoviel MS, Nouraldeen A *et al.* Inhibition of sphingosine 1-phosphate lyase for the treatment of rheumatoid arthritis: discovery of (E)-1-(4-((1R,2S,3R)-1,2,3,4-tetrahydroxybutyl)-1H-imidazol-2-yl)ethanone oxime (LX2931) and (1R,2S,3R)-1-(2-(isoxazol-3-yl)-1H-imidazol-4-yl)butane-1,2,3,4-tetraol (LX2932). *J Med Chem* 2010; **53**: 8650–8662.
83 Kesavan C, Mohan S, Brommage R, Wergedal J. Wnt16 is an important regulator of bone size and the periosteal bone formation response to mechanical loading. *J Bone Miner Res* 2013; **28**(Suppl 1): S100.
84 Skrtic SM *et al.* WNT16 is a novel osteoblast-derived paracrine regulator of osteoclastogenesis, cortical bone mass and fracture susceptibility. *J Bone Miner Res* 2013; **28**(Suppl 1): S39.
85 Motyl KJ, Raetz M, Tekalur SA, Schwartz RC, McCabe LR. CCAAT/enhancer binding protein beta-deficiency enhances type 1 diabetic bone phenotype by increasing marrow adiposity and bone resorption. *Am J Physiol Regul Integr Comp Physiol* 2011; **300**: R1250–R1260.
86 Staiger J, Lueben MJ, Berrigan D *et al.* C/EBPbeta regulates body composition, energy balance-related hormones and tumor growth. *Carcinogenesis* 2009; **30**: 832–840.
87 Tominaga H, Maeda S, Hayashi M *et al.* CCAAT/enhancer-binding protein beta promotes osteoblast differentiation by enhancing Runx2 activity with ATF4. *Mol Biol Cell* 2008; **19**: 5373–5386.
88 Zanotti S, Stadmeyer L, Smerdel-Ramoya A, Durant, D, Canalis E. Misexpression of CCAAT/enhancer binding protein beta causes osteopenia. *J Endocrinol* 2009; **201**: 263–274.
89 Morello R, Bertin TK, Chen Y *et al.* CRTAP is required for prolyl 3-hydroxylation and mutations cause recessive osteogenesis imperfecta. *Cell* 2006; **127**: 291–304.
90 Baldridge D, Lennington J, Weis M *et al.* Generalized connective tissue disease in Crtap$^{-/-}$ mouse. *PLoS One* 2010; **5**: e10560.
91 Weber G, Rabbiosi S, Zamproni I, Fugazzola L. Genetic defects of hydrogen peroxide generation in the thyroid gland. *J Endocrinol Invest* 2013; **36**: 261–266.
92 Johnson KR, Marden CC, Ward-Bailey P, Gagnon LH, Bronson RT, Donahue LR. Congenital hypothyroidism, dwarfism, and hearing impairment caused by a missense mutation in the mouse dual oxidase 2 gene, Duox2. *Mol Endocrinol* 2007; **21:** 1593–1602.
93 Grasberger H, de Deken X, Mayo OB *et al.* Mice deficient in dual oxidase maturation factors are severely hypothyroid. *Mol Endocrinol* 2012; **26**: 481–492.
94 Xing W, Govoni KE, Donahue LR *et al.* Genetic evidence that thyroid hormone is indispensable for prepubertal insulin-like growth factor-I expression and bone acquisition in mice. *J Bone Miner Res* 2012; **27**: 1067–1079.
95 Donko A, Ruisanchez E, Orient A *et al.* Urothelial cells produce hydrogen peroxide through the activation of Duox1. *Free Radic Biol Med* 2010; **49**: 2040–2048.
96 Mackenzie NC, Zhu D, Milne EM *et al.* Altered bone development and an increase in FGF-23 expression in Enpp1($^{-/-}$) mice. *PloS One* 2012; **7**: e32177.
97 Koshizuka Y, Ikegawa S, Sano M, Nakamura K, Nakamura Y. Isolation of novel mouse genes associated with ectopic ossification by differential display method using ttw, a mouse model for ectopic ossification. *Cytogenet Cell Genet* 2001; **94**: 163–168.
98 Babij P, Roudier M, Graves T *et al.* New variants in the *Enpp1* and *Ptpn6* genes cause low BMD, crystal-related arthropathy, and vascular calcification. *J Bone Miner Res* 2009; **24**: 1552–1564.
99 Li Q, Guo H, Chou DW, Berndt A, Sundberg JP, Uitto J. Mutant Enpp1asj mice as a model for generalized arterial calcification of infancy. *Dis Model Mech* 2013; **6**: 1227–1235.
100 Martin A, David V, Quarles LD. Regulation and function of the FGF23/klotho endocrine pathways. *Physiol Rev* 2012; **92**: 131–155.
101 Bhattacharyya N, Chong WH, Gafni RI, Collins MT. Fibroblast growth factor 23: state of the field and future directions. *Trends Endocrinol Metab* 2012; **23**: 610–618.
102 Yamashita T, Yoshitake H, Tsuji K, Kawaguchi N, Nabeshima Y, Noda M. Retardation in bone resorption after bone marrow ablation in klotho mutant mice. *Endocrinology* 2000; **141**: 438–445.
103 Yuan Q, Sato T, Densmore M *et al.* Deletion of PTH rescues skeletal abnormalities and high osteopontin levels in Klotho$^{-/-}$ mice. *PLoS Genet* 2012; **8:** e1002726.
104 Ellwanger K, Saito H, Clément-Lacroix P *et al.* Targeted disruption of the Wnt regulator Kremen induces limb defects and high bone density. *Mol Cell Biol* 2008; **28**: 4875–4882.
105 Schulze J, Seitz S, Saito H *et al.* Negative regulation of bone formation by the transmembrane Wnt antagonist Kremen-2. *PLoS One* 2010; **5**: e10309.
106 Zhou Z, Xie J, Lee D *et al.* Neogenin regulation of BMP-induced canonical Smad signaling and endochondral bone formation. *Dev Cell* 2010; **19**: 90–102.
107 Contie S, Voorzanger-Rousselot N, Litvin J *et al.* Development of a new ELISA for serum periostin: evaluation of growth-related changes and bisphosphonate treatment in mice. *Calcif Tissue Int* 2010; **87**: 341–350.
108 Horiuchi K, Amizuka N, Takeshita S *et al.* Identification and characterization of a novel protein, periostin, with restricted expression to periosteum and periodontal ligament and increased expression by transforming growth factor beta. *J Bone Miner Res* 1999; **14**: 1239–1249.
109 Bonnet N, Standley KN, Bianchi EN *et al.* The matricellular protein periostin is required for sost inhibition and the anabolic response to

mechanical loading and physical activity. *J Biol Chem* 2009; **284**: 35939–35950.

110 Rios H, Koushik SV, Wang H *et al.* Periostin null mice exhibit dwarfism, incisor enamel defects, and an early-onset periodontal disease-like phenotype. *Mol Cell Biol* 2005; **25**: 11131–11144.

111 Bonnet N, Gineyts E, Ammann P, Conway SJ, Garnero P, Ferrari S. Periostin deficiency increases bone damage and impairs injury response to fatigue loading in adult mice. *PLoS One* 2013; **8**: e78347.

112 Fukada T, Civic N, Furuichi T *et al.* The zinc transporter SLC39A13/ZIP13 is required for connective tissue development; its involvement in BMP/TGF-beta signaling pathways. *PLoS One* 2008; **3**: e3642.

113 Giunta C, Elçioglu NH, Albrecht B *et al.* Spondylocheiro dysplastic form of the Ehlers–Danlos syndrome—an autosomal-recessive entity caused by mutations in the zinc transporter gene SLC39A13. *Am J Hum Genet* 2008; **82**: 1290–1305.

114 Shimada T, Kakitani M, Yamazaki Y *et al.* Targeted ablation of Fgf23 demonstrates an essential physiological role of FGF23 in phosphate and vitamin D metabolism. *J Clin Invest* 2004; **113**: 561–568.

115 Chalhoub N, Benachenhou N, Rajapurohitam V *et al.* Grey-lethal mutation induces severe malignant autosomal recessive osteopetrosis in mouse and human. *Nat Med* 2003; **9**: 399–406.

116 Pata M, Heraud C, Vacher J. OSTM1 bone defect reveals an intercellular hematopoietic crosstalk. *J Biol Chem* 2008; **283**: 30522–30530.

117 Lange PF, Wartosch L, Jentsch TJ, Fuhrmann JC. ClC-7 requires Ostm1 as a beta-subunit to support bone resorption and lysosomal function. *Nature* 2006; **440**: 220–223.

118 Chusho H, Tamura N, Ogawa Y *et al.* Dwarfism and early death in mice lacking C-type natriuretic peptide. *Proc Natl Acad Sci USA* 2001; **98**: 4016–4021.

119 Kondo E, Yasoda A, Tsuji T *et al.* Skeletal analysis of the long bone abnormality (lbab/lbab) mouse, a novel chondrodysplastic C-type natriuretic peptide mutant. *Calcif Tissue Int* 2012; **90**: 307–318.

120 Tsuji T, Kunieda T. A loss-of-function mutation in natriuretic peptide receptor 2 (*Npr2*) gene is responsible for disproportionate dwarfism in cn/cn mouse. *J Biol Chem* 2005; **280**: 14288–14292.

121 Sogawa C, Tsuji T, Shinkai Y, Katayama K, Kunieda T. Short-limbed dwarfism: slw is a new allele of Npr2 causing chondrodysplasia. *J Hered* 2007; **98**: 575–580.

122 Bartels CF, Bükülmez H, Padayatti P *et al.* Mutations in the transmembrane natriuretic peptide receptor NPR-B impair skeletal growth and cause acromesomelic dysplasia, type Maroteaux. *Am J Hum Genet* 2004; **75**: 27–34.

123 Miura K, Namba N, Fujiwara M *et al.* An overgrowth disorder associated with excessive production of cGMP due to a gain-of-function mutation of the natriuretic peptide receptor 2 gene. *PLoS One* 2012; **7**: e42180.

124 Dauphinee SM, Eva MM, Yuki KE *et al.* Characterization of two ENU-induced mutations affecting mouse skeletal morphology. *G3 (Bethesda)* 2013; **3**: 1753–1758.

125 Moffatt P, Thomas G, Sellin K *et al.* Osteocrin is a specific ligand of the natriuretic peptide clearance receptor that modulates bone growth. *J Biol Chem* 2007; **282**: 36454–36462.

126 Soriano P, Montgomery C, Geske R, Bradley A. Targeted disruption of the c-src proto-oncogene leads to osteopetrosis in mice. *Cell* 1991; **64**: 693–702.

127 Kubota T, Michigami T, Sakaguchi N *et al.* Lrp6 hypomorphic mutation affects bone mass through bone resorption in mice and impairs interaction with Mesd. *J Bone Miner Res* 2008; **23**: 1661–1671.

128 Mani A, Radhakrishnan J, Wang H *et al.* LRP6 mutation in a family with early coronary disease and metabolic risk factors. *Science* 2007; **315**: 1278–1282.

129 Babij P, Zhao W, Small C *et al.* High bone mass in mice expressing a mutant LRP5 gene. *J Bone Miner Res* 2003; **18**: 960–974.

130 Boyden LM, Mao J, Belsky J *et al.* High bone density due to a mutation in LDL-receptor-related protein 5. *N Engl J Med* 2002; **346**: 1513–1521.

131 MacDonald BT, Joiner DM, Oyserman SM *et al.* Bone mass is inversely proportional to Dkk1 levels in mice. *Bone* 2007; **41**: 331–339.

132 Morvan F, Boulukos K, Clément-Lacroix P *et al.* Deletion of a single allele of the Dkk1 gene leads to an increase in bone formation and bone mass. *J Bone Miner Res* 2006; **21**: 934–945.

133 Morse A, Frank C, Kelly NH *et al.* Sclerostin null and dickkopf-1 null mice show an increased response to mechanical loading. *Proc Orthop Res Soc Annu Meet* 2014; Poster Number 0567.

134 McDonald M, Morse M, Baldock P *et al.* Homozygous deletion of Dickkopf1 results in a high bone mass phenotype. *J Bone Miner Res* 2010; **25**(Suppl 1): S23–S24.

135 Li J, Sarosi I, Cattley RC *et al.* Dkk1-mediated inhibition of Wnt signaling in bone results in osteopenia. *Bone* 2006; **39**: 754–766.

136 Fulciniti M, Tassone P, Hideshima T *et al.* Anti-DKK1 mAb (BHQ880) as a potential therapeutic agent for multiple myeloma. *Blood* 2009; **114**: 371–379.

137 Glantschnig H, Hampton RA, Lu P *et al.* Generation and selection of novel fully human monoclonal antibodies that neutralize Dickkopf-1 (DKK1) inhibitory function in vitro and increase bone mass *in vivo*. *J Biol Chem* 2010; **285**: 40135–40147.

138 Glantschnig H, Scott K, Hampton R *et al.* A rate-limiting role for Dickkopf-1 in bone formation and the remediation of bone loss in mouse and primate models of postmenopausal osteoporosis by an experimental therapeutic antibody. *J Pharmacol Exp Ther* 2011; **338**: 568–578.

139 Ke HZ, Richards WG, Li X, Ominsky MS. Sclerostin and Dickkopf-1 as therapeutic targets in bone diseases. *Endocr Rev* 2012; **33**: 747–783.

140 Pozzi S, Fulciniti M, Yan H *et al. In vivo* and *in vitro* effects of a novel anti-Dkk1 neutralizing antibody in multiple myeloma. *Bone* 2013; **53**: 487–496.

141 Zhou F, Meng S, Song H, Claret FX. Dickkopf-1 is a key regulator of myeloma bone disease: opportunities and challenges for therapeutic intervention. *Blood Rev* 2013; **27**: 261–267.

142 Fan W, *et al.* Differential impact of Dkk1 neutralizing antibodies on Wnt signaling and bone mineral density. *J Bone Miner Res* 2011; **26**(Suppl 1): S117.

143 Li X, Grisanti M, Fan W *et al.* Dickkopf-1 regulates bone formation in young growing rodents and upon traumatic injury. *J Bone Miner Res* 2011; **26**: 2610–2621.

144 Mukhopadhyay M, Gorivodsky M, Shtrom S *et al.* Dkk2 plays an essential role in the corneal fate of the ocular surface epithelium. *Development* 2006; **133**: 2149–2154.

145 Gage PJ, Qian M, Wu D, Rosenberg KI. The canonical Wnt signaling antagonist DKK2 is an essential effector of PITX2 function during normal eye development. *Dev Biol* 2008; **317**: 310–324.

146 Li X, Liu P, Liu W *et al.* Dkk2 has a role in terminal osteoblast differentiation and mineralized matrix formation. *Nat Genet* 2005; **37**: 945–952.

147 Barrantes Idel B, Montero-Pedrazuela A, Guadaño-Ferraz A, *et al.* Generation and characterization of dickkopf3 mutant mice. *Mol Cell Biol* 2006; **26**: 2317–2326.

148 Ouchi N, Higuchi A, Ohashi K *et al.* Sfrp5 is an anti-inflammatory adipokine that modulates metabolic dysfunction in obesity. *Science* 2010; **329**: 454–457.

149 Mori H, Prestwich TC, Reid MA *et al.* Secreted frizzled-related protein 5 suppresses adipocyte mitochondrial metabolism through WNT inhibition. *J Clin Invest* 2012; **122**: 2405–2416.

150 Cox S, Smith L, Bogani D, Cheeseman M, Siggers P, Greenfield A. Sexually dimorphic expression of secreted frizzled-related (SFRP) genes in the developing mouse Mullerian duct. *Mol Reprod Dev* 2006; **73**: 1008–1016.

151 Satoh W, Gotoh T, Tsunematsu Y, Aizawa S, Shimono A. Sfrp1 and Sfrp2 regulate anteroposterior axis elongation and somite segmentation during mouse embryogenesis. *Development* 2006; **133**: 989–999.

152 Morello R, Bertin TK, Schlaubitz S *et al.* Brachy-syndactyly caused by loss of Sfrp2 function. *J Cell Physiol* 2008; **217**: 127–137.

153 Yao W, Cheng Z, Shahnazari M, Dai W, Johnson ML, Lane NE. Overexpression of secreted frizzled-related protein 1 inhibits bone formation and attenuates parathyroid hormone bone anabolic effects. *J Bone Miner Res* 2010; **25**: 190–199.

154 Bodine PV, Zhao W, Kharode YP *et al.* The Wnt antagonist secreted frizzled-related protein-1 is a negative regulator of trabecular bone formation in adult mice. *Mol Endocrinol* 2004; **18**: 1222–1237.

155 Bodine PV, Seestaller-Wehr L, Kharode YP, Bex FJ, Komm BS. Bone anabolic effects of parathyroid hormone are blunted by deletion of the Wnt antagonist secreted frizzled-related protein-1. *J Cell Physiol* 2007; **210**: 352–357.

156 Joesting MS, Cheever TR, Volzing KG *et al.* Secreted frizzled related protein 1 is a paracrine modulator of epithelial branching morphogenesis, proliferation, and secretory gene expression in the prostate. *Dev Biol* 2008; **317**: 161–173.

157 Gauger KJ, Bassa LM, Henchey EM *et al.* Mice deficient in sfrp1 exhibit increased adiposity, dysregulated glucose metabolism, and enhanced macrophage infiltration. *PloS One* 2013; **8**: e78320.

158 Lories RJ, Peeters J, Bakker A *et al.* Articular cartilage and biomechanical properties of the long bones in Frzb-knockout mice. *Arthritis Rheum* 2007; **56**: 4095–4103.

159 Baker-Lepain JC, Lynch JA, Parimi N *et al.* Variant alleles of the Wnt antagonist FRZB are determinants of hip shape and modify the relationship between hip shape and osteoarthritis. *Arthritis Rheum* 2012; **64**: 1457–1465.

160 Saito H, Wissmann C, Suzuki H *et al.* Deletion of the Wnt signaling antagonist Secreted frizzled related protein 4 (sFRP4) in mice induces opposite bone formation phenotypes in trabecular and cortical bone. *J Bone Miner Res* 2008; **23**(Suppl 1) : S3.

161 Kao R, Louie A, Lu WD, Nissenson R. Differential regulation of cortical and trabecular bone by Secreted frizzled-related protein 4 (Sfrp4). *J Bone Miner Res* 2010; **25**(Suppl 1): S425.

162 Saito H, *et al.* sFrp4 differentially regulates trabecular and cortical bone mass via canonical Wnt and Ror2-BMP-sclerostin signaling, respectively. *J Bone Miner Res* 2011; **26**(Suppl 1): S50.

163 Kansara M, Tsang M, Kodjabachian L *et al.* Wnt inhibitory factor 1 is epigenetically silenced in human osteosarcoma, and targeted disruption accelerates osteosarcomagenesis in mice. *J Clin Invest* 2009; **119**: 837–851.

164 Schaniel C, Sirabella D, Qiu J, Niu X, Lemischka IR, Moore KA. Wnt-inhibitory factor 1 dysregulation of the bone marrow niche exhausts hematopoietic stem cells. *Blood* 2011; **118**: 2420–2429.

165 Cawthorn WP, Bree AJ, Yao Y *et al.* Wnt6, Wnt10a and Wnt10b inhibit adipogenesis and stimulate osteoblastogenesis through a beta-catenin-dependent mechanism. *Bone* 2012; **50**: 477–489.

166 Mak W, Shao X, Dunstan CR, Seibel MJ, Zhou H. Biphasic glucocorticoid-dependent regulation of Wnt expression and its inhibitors in mature osteoblastic cells. *Calcif Tissue Int* 2009; **85**: 538–545.

167 Wend P, Wend K, Krum SA, Miranda-Carboni GA. The role of WNT10B in physiology and disease. *Acta Physiol (Oxf)* 2012; **204**: 34–51.

168 Stevens JR, Miranda-Carboni GA, Singer MA, Brugger SM, Lyons KM, Lane TF. Wnt10b deficiency results in age-dependent loss of bone mass and progressive reduction of mesenchymal progenitor cells. *J Bone Miner Res* 2010; **25**: 2138–2147.

169 Bennett CN, Longo KA, Wright WS *et al.* Regulation of osteoblastogenesis and bone mass by Wnt10b. *Proc Natl Acad Sci USA* 2005; **102**: 3324–3329.

170 Bennett CN, Ouyang H, Ma YL *et al.* Wnt10b increases postnatal bone formation by enhancing osteoblast differentiation. *J Bone Miner Res* 2007; **22**: 1924–1932.

171 Terauchi M, Li JY, Bedi B *et al.* T lymphocytes amplify the anabolic activity of parathyroid hormone through Wnt10b signaling. *Cell Metab* 2009; **10**: 229–240.

172 Kukita T, Wada N, Kukita A *et al.* RANKL-induced DC-STAMP is essential for osteoclastogenesis. *J Exp Med* 2004; **200**: 941–946.

173 Yagi M, Miyamoto T, Sawatani Y *et al.* DC-STAMP is essential for cell–cell fusion in osteoclasts and foreign body giant cells. *J Exp Med* 2005; **202**: 345–351.

174 Miyamoto T. Regulators of osteoclast differentiation and cell–cell fusion. *Keio J* Med 2011; **60**: 101–105.

175 Kollmann K, Pestka JM, Kühn SC *et al.* Decreased bone formation and increased osteoclastogenesis cause bone loss in mucolipidosis II. *EMBO Mol Med* 2013; **5**: 1871–1886.

176 Gelfman CM, Vogel P, Issa TM *et al.* Mice lacking alpha/beta subunits of GlcNAc-1-phosphotransferase exhibit growth retardation, retinal degeneration, and secretory cell lesions. *Invest Ophthalmol Vis Sci* 2007; **48**: 5221–5228.

177 Vogel P, Payne BJ, Read R *et al.* Comparative pathology of murine mucolipidosis types II and IIIC. *Vet Pathol* 2009; **46**: 313–324.

178 Colledge WH. Transgenic mouse models to study Gpr54/kisspeptin physiology. *Peptides* 2009; **30**: 34–41.

179 Dungan Lemko HM, Elias CF. Kiss of the mutant mouse: how genetically altered mice advanced our understanding of kisspeptin's role in reproductive physiology. *Endocrinology* 2012; **153**: 5119–5129.

180 Brommage R, Qian N, Vogel P *et al.* Mice failing to undergo puberty due to targeted inactivation of the GPR54 gene exhibit alterations in body composition and reduced bone mass. *J Bone Miner Res* 2004; **19**(Suppl 1): S93.

181 Hamrick MW, Samaddar T, Pennington C, McCormick J. Increased muscle mass with myostatin deficiency improves gains in bone strength with exercise. *J Bone Miner Res* 2006; **21**: 477–483.

182 Elkasrawy MN, Hamrick MW. Myostatin (GDF-8) as a key factor linking muscle mass and bone structure. *J Musculoskelet Neuronal Interact* 2010; **10**: 56–63.

183 Mitchell AD, Wall RJ. *In vivo* evaluation of changes in body composition of transgenic mice expressing the myostatin pro domain using dual energy X-ray absorptiometry. *Growth Dev Aging* 2007; **70**: 25–37.

184 Inoue K, Matsuda K, Itoh M *et al.* Osteopenia and male-specific sudden cardiac death in mice lacking a zinc transporter gene, Znt5. *Hum Mol Genet* 2002; **11**: 1775–1784.

185 Dacquin R, Davey RA, Laplace C *et al.* Amylin inhibits bone resorption while the calcitonin receptor controls bone formation *in vivo*. *J Cell Biol* 2004; **164**: 509–514.

186 Davey RA, Turner AG, McManus JF *et al.* Calcitonin receptor plays a physiological role to protect against hypercalcemia in mice. *J Bone Miner Res* 2008; **23**: 1182–1193.

187 Gazzerro E, Smerdel-Ramoya A, Zanotti S *et al.* Conditional deletion of gremlin causes a transient increase in bone formation and bone mass. *J Biol Chem* 2007; **282**: 31549–31557.

188 Canalis E, Parker K, Zanotti S. Gremlin1 is required for skeletal development and postnatal skeletal homeostasis. *J Cell Physiol* 2012; **227**: 269–277.

189 Cheung CL, Lau KS, Sham PC, Tan KC, Kung AW. Genetic variants in GREM2 are associated with bone mineral density in a southern Chinese population. *J Clin Endocrinol Metab* 2013; **98**: E1557–E1561.

190 Paternoster L, Lorentzon M, Lehtimäki T *et al.* Genetic determinants of trabecular and cortical volumetric bone mineral densities and bone microstructure. *PLoS Genet* 2013; **9**: e1003247.

191 Zuniga E, Rippen M, Alexander C, Schilling TF, Crump JG. Gremlin 2 regulates distinct roles of BMP and Endothelin 1 signaling in dorsoventral patterning of the facial skeleton. *Development* 2011; **138**: 5147–5156.

192 Vogel P, Liu J, Platt KA *et al.* Malformation of incisor teeth in Grem2$^{-/-}$ mice. *Vet Pathol* 2014; [Epub ahead of print].

193 Poli V, Balena R, Fattori E *et al.* Interleukin-6 deficient mice are protected from bone loss caused by estrogen depletion. *EMBO J* 1994; **13**: 1189–1196.

194 Dai J, Lin D, Zhang J *et al.* Chronic alcohol ingestion induces osteoclastogenesis and bone loss through IL-6 in mice. *J Clin Invest* 2000; **106**: 887–895.

195 Jilka RL, Hangoc G, Girasole G *et al.* Increased osteoclast development after estrogen loss: mediation by interleukin-6. *Science* 1992; **257**: 88–91.

196 Kimble RB, Bain S, Pacifici R. The functional block of TNF but not of IL-6 prevents bone loss in ovariectomized mice. *J Bone Miner Res* 1997; **12**: 935–941.

197 O'Brien CA, Jilka RL, Fu Q, Stewart S, Weinstein RS, Manolagas SC. IL-6 is not required for parathyroid hormone stimulation of RANKL expression, osteoclast formation, and bone loss in mice. *Am J Physiol Endocrinol Metab* 2005; **289**: E784–E793.

198 del Fattore A, Cappariello A, Capulli M *et al.* An experimental therapy to improve skeletal growth and prevent bone loss in a mouse model overexpressing IL-6. *Osteoporos Int* 2014; **25**: 681–692.

199 Grey A, Mitnick MA, Masiukiewicz U *et al.* A role for interleukin-6 in parathyroid hormone-induced bone resorption *in vivo*. *Endocrinology* 1999; **140**: 4683–4690.

200 Xu J, Song P, Nakamura S *et al.* Deletion of the chloride transporter slc26a7 causes distal renal tubular acidosis and impairs gastric acid secretion. *J Biol Chem* 2009; **284**: 29470–29479.

201 Spitzweg C, Morris JC. Genetics and phenomics of hypothyroidism and goiter due to NIS mutations. *Mol Cell Endocrinol* 2010; **322**: 56–63.

202 Everett LA, Belyantseva IA, Noben-Trauth K *et al.* Targeted disruption of mouse Pds provides insight about the inner-ear defects encountered in Pendred syndrome. *Hum Mol Genet* 2001; **10**: 153–161.

203 Kim KX, Sanneman JD, Kim HM *et al.* Slc26a7 chloride channel activity and localization in mouse Reissner's membrane epithelium. *PLoS One* 2014; **9**: e97191.

204 Khadeer MA, Sahu SN, Bai G, Abdulla S, Gupta A. Expression of the zinc transporter ZIP1 in osteoclasts. *Bone* 2005; **37**: 296–304.

205 Kambe T, Geiser J, Lahner B, Salt DE, Andrews GK. Slc39a1 to 3 (subfamily II) Zip genes in mice have unique cell-specific functions during adaptation to zinc deficiency. *Am J Physiol Regul Integr Comp Physiol* 2008; **294**: R1474–R1481.

206 Gilmour DT, Lyon GJ, Carlton MB *et al.* Mice deficient for the secreted glycoprotein SPARC/osteonectin/BM40 develop normally but show severe age-onset cataract formation and disruption of the lens. *EMBO J* 1998; **17**: 1860–1870.

207 Norose K, Clark JI, Syed NA *et al.* SPARC deficiency leads to early-onset cataractogenesis. *Invest Ophthalmol Vis Sci* 1998; **39**: 2674–2680.

208 Bradshaw AD, Graves DC, Motamed K, Sage EH. SPARC-null mice exhibit increased adiposity without significant differences in overall body weight. *Proc Natl Acad Sci USA* 2003; **100**: 6045–6050.

209 Gruber HE, Sage EH, Norton HJ *et al.* Targeted deletion of the SPARC gene accelerates disc degeneration in the aging mouse. *J Histochem Cytochem* 2005; **53**: 1131–1138.

210 Delany AM, Amling M, Priemel M *et al.* Osteopenia and decreased bone formation in osteonectin-deficient mice. *J Clin Invest* 2000; **105**: 1325.

211 Boskey AL, Moore DJ, Amling M, Canalis E, Delany AM. Infrared analysis of the mineral and matrix in bones of osteonectin-null mice and their wildtype controls. *J Bone Miner Res* 2003; **18**: 1005–1011.

212 Mansergh FC, Wells T, Elford C *et al.* Osteopenia in Sparc (osteonectin)-deficient mice: characterization of phenotypic determinants of femoral strength and changes in gene expression. *Physiol Genomics* 2007; **32**: 64–73.

213 Barros NM, Hoac B, Neves RL *et al.* Proteolytic processing of osteopontin by PHEX and accumulation of osteopontin fragments in Hyp mouse bone, the murine model of X-linked hypophosphatemia. *J Bone Miner Res* 2013; **28**: 688–699.

214 Ishijima M, Rittling SR, Yamashita T *et al.* Enhancement of osteoclastic bone resorption and suppression of osteoblastic bone formation in response to reduced mechanical stress do not occur in the absence of osteopontin. *J Exp Med* 2001; **193**: 399–404.

215 Boskey AL, Spevak L, Paschalis E, Doty SB, McKee MD. Osteopontin deficiency increases mineral content and mineral crystallinity in mouse bone. *Calcif Tissue Int* 2002; **71**: 145–154.

216 Ono N, Nakashima K, Rittling SR *et al.* Osteopontin negatively regulates parathyroid hormone receptor signaling in osteoblasts. *J Biol Chem* 2008; **283**: 19400–19409.

217 Yoshitake H, Rittling SR, Denhardt DT, Noda M. Osteopontin-deficient mice are resistant to ovariectomy-induced bone resorption. *Proc Natl Acad Sci USA* 1999; **96**: 8156–8160.

218 Harmey D, Johnson KA, Zelken J *et al.* Elevated skeletal osteopontin levels contribute to the hypophosphatasia phenotype in Akp2($^{-/-}$) mice. *J Bone Miner Res* 2006; **21**: 1377–1386.

219 Malaval L, Wade-Guéye NM, Boudiffa M *et al.* Bone sialoprotein plays a functional role in bone formation and osteoclastogenesis. *J Exp Med* 2008; **205**: 1145–1153.

220 Thurner PJ, Chen CG, Ionova-Martin S *et al.* Osteopontin deficiency increases bone fragility but preserves bone mass. *Bone* 2010; **46**: 1564–1573.

221 Novack DV, Faccio R. Osteoclast motility: putting the brakes on bone resorption. *Ageing Res Rev* 2011; **10**: 54–61.

222 Sakai D, Tong HS, Minkin C. Osteoclast molecular phenotyping by random cDNA sequencing. *Bone* 1995; **17**: 111–119.

223 Shuang F, Sun Y, Yang HH *et al.* Destrin deletion enhances the bone loss in hindlimb suspended mice. *Eur J Appl Physiol* 2013; **113:** 403–410.

224 Niwa R, Nagata-Ohashi K, Takeichi M, Mizuno K, Uemura T. Control of actin reorganization by Slingshot, a family of phosphatases that dephosphorylate ADF/cofilin. *Cell* 2002; **108**: 233–246.

225 Blangy A, Touaitahuata H, Cres G, Pawlak G. Cofilin activation during podosome belt formation in osteoclasts. *PLoS One* 2012; **7**: e45909.

226 Mizuno K. Signaling mechanisms and functional roles of cofilin phosphorylation and dephosphorylation. *Cell Signal* 2013; **25**: 457–469.

227 Meng Y, Zhang Y, Tregoubov V *et al.* Abnormal spine morphology and enhanced LTP in LIMK-1 knockout mice. *Neuron* 2002; **35**: 121–133.

228 Kawano T, Zhu M, Troiano N *et al.* LIM kinase 1 deficient mice have reduced bone mass. *Bone* 2013; **52**: 70–82.

229 Collette NM, Yee CS, Murugesh D *et al.* Sost and its paralog Sostdc1 coordinate digit number in a Gli3-dependent manner. *Dev Biol* 2013; **383:** 90–105.

230 Ellies DL, Economou A, Viviano B *et al.* Wise regulates bone deposition through genetic interactions with Lrp5. *PLoS One* 2014; **9**: e96257.

231 Person AD, Beiraghi S, Sieben CM *et al.* WNT5A mutations in patients with autosomal dominant Robinow syndrome. *Dev Dyn* 2010; **239**: 327–337.

232 Yamaguchi TP, Bradley A, McMahon AP, Jones S. A Wnt5a pathway underlies outgrowth of multiple structures in the vertebrate embryo. *Development* 1999; **126**: 1211–1223.

233 Lin M, Li L, Liu C *et al.* Wnt5a regulates growth, patterning, and odontoblast differentiation of developing mouse tooth. *Dev Dyn* 2011; **240**: 432–440.

234 Yang Y, Topol L, Lee H, Wu J. Wnt5a and Wnt5b exhibit distinct activities in coordinating chondrocyte proliferation and differentiation. *Development* 2003; **130**: 1003–1015.

235 Maeda K, Kobayashi Y, Udagawa N *et al.* Wnt5a-Ror2 signaling between osteoblast-lineage cells and osteoclast precursors enhances osteoclastogenesis. *Nat Med* 2012; **18**: 405–412.

236 Agalliu D, Takada S, Agalliu I, McMahon AP, Jessell TM. Motor neurons with axial muscle projections specified by Wnt4/5 signaling. *Neuron* 2009; **61**: 708–720.

237 DeWitt MR, Chen P, Aschner M. Manganese efflux in Parkinsonism: insights from newly characterized SLC30A10 mutations. *Biochem Biophys Res Commun* 2013; **432**: 1–4.

238 Alam I, Gray AK, Chu K *et al.* Generation of the first autosomal dominant osteopetrosis type II (ADO2) disease models. *Bone* 2014; **59**: 66–75.

239 Rajan I, Read R, Small, DL, Perrard J, Vogel P. An alternative splicing variant in Clcn7$^{-/-}$ mice prevents osteopetrosis but not neural and retinal degeneration. *Vet Pathol* 2011; **48**: 663–675.

240 Kornak U, Kasper D, Bösl MR *et al.* Loss of the ClC-7 chloride channel leads to osteopetrosis in mice and man. *Cell* 2001; **104**: 205–215.

241 Neutzsky-Wulff AV, Karsdal MA, Henriksen K. Characterization of the bone phenotype in ClC-7-deficient mice. *Calcif Tissue Int* 2008; **83**: 425–437.

242 Vega RB, Matsuda K, Oh J *et al.* Histone deacetylase 4 controls chondrocyte hypertrophy during skeletogenesis. *Cell* 2004; **119**: 555–566.

243 Arnold MA, Kim Y, Czubryt MP *et al.* MEF2C transcription factor controls chondrocyte hypertrophy and bone development. *Dev Cell* 2007; **12**: 377–389.

244 Rajan I, Savelieva KV, Ye GL *et al.* Loss of the putative catalytic domain of HDAC4 leads to reduced thermal nociception and seizures while allowing normal bone development. *PloS One* 2009; **4**: e6612.

245 van Wesenbeeck L, Odgren PR, Coxon FP *et al.* Involvement of PLEKHM1 in osteoclastic vesicular transport and osteopetrosis in incisors absent rats and humans. *J Clin Invest* 2007; **117**: 919–930.

246 del Fattore A, Fornari R, Van Wesenbeeck L *et al.* A new heterozygous mutation (R714C) of the osteopetrosis gene, pleckstrin homolog domain containing family M (with run domain) member 1 (PLEKHM1), impairs vesicular acidification and increases TRACP secretion in osteoclasts. *J Bone Miner Res* 2008; **23**: 380–391.

247 Vogel P, Read RW, Hansen GM *et al.* Congenital hydrocephalus in genetically engineered mice. *Vet Pathol* 2012; **49**: 166–181.

248 Ueda Y, Yamaguchi R, Ikawa M *et al.* PGAP1 knock-out mice show otocephaly and male infertility. *J Biol Chem* 2007; **282**: 30373–30380.

249 McKean DM, Niswander L. Defects in GPI biosynthesis perturb Cripto signaling during forebrain development in two new mouse models of holoprosencephaly. *Biol Open* 2012; **1**: 874–883.

250 Park J, Kang SI, Lee SY *et al.* Tumor suppressor ras association domain family 5 (RASSF5/NORE1) mediates death receptor ligand-induced apoptosis. *J Biol Chem* 2010; **285**: 35029–35038.

251 Kondo Y, Inai Y, Sato Y *et al.* Senescence marker protein 30 functions as gluconolactonase in L-ascorbic acid biosynthesis, and its knockout mice are prone to scurvy. *Proc Natl Acad Sci USA* 2006; **103**: 5723–5728.

252 Maeda N, Hagihara H, Nakata Y *et al.* Aortic wall damage in mice unable to synthesize ascorbic acid. *Proc Natl Acad Sci USA* 2000; **97**: 841–846.

253 Kawai T, Nishikimi M, Ozawa T, Yagi K. A missense mutation of L-gulono-gamma-lactone oxidase causes the inability of scurvy-prone osteogenic disorder rats to synthesize L-ascorbic acid. *J Biol Chem* 1992; **267**: 21973–21976.

254 Beamer WG, Rosen CJ, Bronson RT *et al.* Spontaneous fracture (sfx): a mouse genetic model of defective peripubertal bone formation. *Bone* 2000; **27**: 619–626.

255 Mohan S, Kapoor A, Singgih A *et al.* Spontaneous fractures in the mouse mutant sfx are caused by deletion of the gulonolactone oxidase gene, causing vitamin C deficiency. *J Bone Miner Res* 2005; **20**: 1597–1610.

256 Gabbay KH, Bohren KM, Morello R, Bertin T, Liu J, Vogel P. Ascorbate synthesis pathway: dual role of ascorbate in bone homeostasis. *J Biol Chem* 2010; **285**: 19510–19520.

257 Opsahl Vital S, Gaucher C, Bardet C *et al.* Tooth dentin defects reflect genetic disorders affecting bone mineralization. *Bone* 2012; **50**: 989–997.

258 Foster BL, Ramnitz MS, Gafni RI *et al.* Rare bone diseases and their dental, oral, and craniofacial manifestations. *J Dent Res* 2014; **93**: 7S–19S.

259 Al-Douri SM, Johnson DR. The development of the teeth of the microphthalmic (mi/mi) mouse. *J Anat* 1987; **153**: 139–149.

260 Ma D, Zhang R, Sun Y *et al.* A novel role of periostin in postnatal tooth formation and mineralization. *J Biol Chem* 2011; **286**: 4302–4309.

261 Kassai Y, Munne P, Hotta Y *et al.* Regulation of mammalian tooth cusp patterning by ectodin. *Science* 2005; **309**: 2067–2070.

262 Ahn Y, Sanderson BW, Klein OD, Krumlauf R. Inhibition of Wnt signaling by Wise (Sostdc1) and negative feedback from Shh controls tooth number and patterning. *Development* 2010; **137**: 3221–3231.

263 Miyata A, Baba O, Oda T, Ishikawa I, Takano Y. Diverse effects of c-src deficiency on molar tooth development and eruption in mice. *Arch Histol Cytol* 2007; **70**: 63–78.

264 Savelieva KV, Zhao S, Pogorelov VM *et al.* Genetic disruption of both tryptophan hydroxylase genes dramatically reduces serotonin and affects behavior in models sensitive to antidepressants. *PloS One* 2008; **3**: e3301.

265 Walther DJ, Peter JU, Bashammakh S *et al.* Synthesis of serotonin by a second tryptophan hydroxylase isoform. *Science* 2003; **299**: 76.

266 Liu Q, Yang Q, Sun W *et al.* Discovery and characterization of novel tryptophan hydroxylase inhibitors that selectively inhibit serotonin synthesis in the gastrointestinal tract. *J Pharmacol Exp Ther* 2008; **325**: 47–55.

267 Yadav VK, Oury F, Suda N *et al.* A serotonin-dependent mechanism explains the leptin regulation of bone mass, appetite, and energy expenditure. *Cell* 2009; **138**: 976–989.

268 Shi ZC, Devasagayaraj A, Gu K *et al.* Modulation of peripheral serotonin levels by novel tryptophan hydroxylase inhibitors for the potential treatment of functional gastrointestinal disorders. *J Med Chem* 2008; **51**: 3684–3687.

269 Jin H, Cianchetta G, Devasagayaraj A *et al.* Substituted 3-(4-(1,3,5-triazin-2-yl)-phenyl)-2-aminopropanoic acids as novel tryptophan hydroxylase inhibitors. *Bioorg Med Chem Lett* 2009; **19**: 5229–5232.

270 Cianchetta G, Stouch T, Yu W *et al.* Mechanism of inhibition of novel tryptophan hydroxylase inhibitors revealed by co-crystal structures and kinetic analysis. *Curr Chem Genomics* 2010; **4**: 19–26.

271 Brown PM, Drossman DA, Wood AJ *et al.* The tryptophan hydroxylase inhibitor LX1031 shows clinical benefit in patients with nonconstipating irritable bowel syndrome. *Gastroenterology* 2011; **141**: 507–516.

272 Brommage R, Smith DD, Liu J, Yu W, Yang QM, Powell DR. Genetic disruption of brain serotonin content in mice produces leanness with hyperphagia and elevated physical activity but minimal skeletal changes. *F1000Posters* 2014; **5**: 1029.

273 Wu J, Glimcher LH, Aliprantis AO. HCO3-/Cl- anion exchanger SLC4A2 is required for proper osteoclast differentiation and function. *Proc Natl Acad Sci USA* 2008; **105**: 16934–16939.

274 Jansen ID, Mardones P, Lecanda F *et al.* Ae2(a,b)-deficient mice exhibit osteopetrosis of long bones but not of calvaria. *FASEB J* 2009; **23**: 3470–3481.

275 Cortes VA, Curtis DE, Sukumaran S *et al.* Molecular mechanisms of hepatic steatosis and insulin resistance in the AGPAT2-deficient mouse model of congenital generalized lipodystrophy. *Cell Metab* 2009; **9**: 165–176.

276 Vogel P, Read R, Hansen G *et al.* Pathology of congenital generalized lipodystrophy in Agpat2$^{-/-}$ mice. *Vet Pathol* 2011; **48**: 642–654.

277 Settembre C, Annunziata I, Spampanato C *et al.* Systemic inflammation and neurodegeneration in a mouse model of multiple sulfatase deficiency. *Proc Natl Acad Sci USA* 2007; **104**: 4506–4511.

278 Settembre C, Arteaga-Solis E, McKee M *et al.* Proteoglycan desulfation determines the efficiency of chondrocyte autophagy and the extent of FGF signaling during endochondral ossification. *Genes Dev* 2008; **22**: 2645–2650.

279 Kim JS, Ryoo ZY, Chun JS. Cytokine-like 1 (Cytl1) regulates the chondrogenesis of mesenchymal cells. *J Biol Chem* 2007; **282**: 29359–29367.

280 Jeon J, Oh H, Lee G *et al.* Cytokine-like 1 knock-out mice (Cytl1$^{-/-}$) show normal cartilage and bone development but exhibit augmented osteoarthritic cartilage destruction. *J Biol Chem* 2011; **286**: 27206–27213.

281 Doetschman T. Influence of genetic background on genetically engineered mouse phenotypes. *Methods Mol Biol* 2009; **530**: 423–433.

282 Matthaei KI. Identification of therapeutic drug targets through genetically manipulated mice: are we getting it right? *Pharmacol Ther* 2009; **123:** 32–36.

283 Keane TM, Goodstadt L, Danecek P *et al.* Mouse genomic variation and its effect on phenotypes and gene regulation. *Nature* 2011; **477**: 289–294.

284 Hofmann WE, Liu X, Bearden CM, Harper ME, Kozak LP. Effects of genetic background on thermoregulation and fatty acid-induced uncoupling of mitochondria in UCP1-deficient mice. *J Biol Chem* 2001; **276**: 12460–12465.

285 Qiu J, Ogus S, Mounzih K, Ewart-Toland A, Chehab FF. Leptin-deficient mice backcrossed to the BALB/cJ genetic background have reduced adiposity, enhanced fertility, normal body temperature, and severe diabetes. *Endocrinology* 2001; **142**: 3421–3425.

286 Toye AA, Lippiat JD, Proks P *et al.* A genetic and physiological study of impaired glucose homeostasis control in C57BL/6J mice. *Diabetologia* 2005; **48**: 675–686.

287 Freeman HC, Hugill A, Dear NT, Ashcroft FM, Cox RD. Deletion of nicotinamide nucleotide transhydrogenase: a new quantitive trait locus accounting for glucose intolerance in C57BL/6J mice. *Diabetes* 2006; **55**: 2153–2156.

288 Scudamore CL. Integrating pathology into human disease modelling--how to eat the elephant. *Dis Model Mech* 2014; **7**: 495–497.

289 Adissu HA, Estabel J, Sunter D *et al.* Histopathology reveals correlative and unique phenotypes in a high-throughput mouse phenotyping screen. *Dis Model Mech* 2014; **7**: 515–524.

290 Prinz F, Schlange T, Asadullah K. Believe it or not: how much can we rely on published data on potential drug targets? *Nat Rev Drug Discov* 2011; **10**: 712.

291 Begley CG, Ellis LM. Drug development: Raise standards for preclinical cancer research. *Nature* 2012; **483**: 531–533.

292 Collins FS, Tabak LA. Policy: NIH plans to enhance reproducibility. *Nature* 2014; **505**: 612–613.

293 Boskey AL, van der Meulen MC, Wright TM. Guidelines for describing mouse skeletal phenotype. *J Orthop Res* 2003; **21**: 1–5.

294 Manolagas SC, Kronenberg HM. Reproducibility of results in preclinical studies: a perspective from the bone field. *J Bone Miner Res* 2014; **29**: 2131–2140.

295 Brommage R, Jeter-Jones S, Xiong WC, Champ R, Liu J. Mouse femoral neck architecture determined by microCT reflects skeletal architecture observed at other bone sites. *J Bone Miner Res* 2013; **28**(Suppl 1): S347–S348.

296 Malloy PJ, Feldman D. The role of vitamin D receptor mutations in the development of alopecia. *Mol Cell Endocrinol* 2011; **347**: 90–96.

297 Demay MB, MacDonald PN, Skorija K, Dowd DR, Cianferotti L, Cox M. Role of the vitamin D receptor in hair follicle biology. *J Steroid Biochem Mol Biol* 2007; **103**: 344–346.

298 Barbaric I, Miller G, Dear TN. Appearances can be deceiving: phenotypes of knockout mice. *Brief Funct Genomic Proteomic* 2007; **6**: 91–103.

299 Nagase S, Shimamune K, Shumiya S. Albumin-deficient rat mutant. *Science* 1979; **205**: 590–591.

300 Kutuzova GD, Akhter S, Christakos S, Vanhooke J, Kimmel-Jehan C, Deluca HF. Calbindin D(9k) knockout mice are indistinguishable from wild-type mice in phenotype and serum calcium level. *Proc Natl Acad Sci USA* 2006; **103**: 12377–12381.

301 Lee GS, Lee KY, Choi KC *et al.* Phenotype of a calbindin-D9k gene knockout is compensated for by the induction of other calcium transporter genes in a mouse model. *J Bone Miner Res* 2007; **22**: 1968–1978.

302 Akhter S, Kutuzova GD, Christakos S, DeLuca HF. Calbindin D9k is not required for 1,25-dihydroxyvitamin D3-mediated Ca^{2+} absorption in small intestine. *Arch Biochem Biophys* 2007; **460**: 227–232.

303 Kutuzova GD, Sundersingh F, Vaughan J *et al.* TRPV6 is not required for 1alpha,25-dihydroxyvitamin D3-induced intestinal calcium absorption *in vivo*. *Proc Natl Acad Sci USA* 2008; **105**: 19655–19659.

304 Yngvadottir B, Xue Y, Searle S *et al.* A genome-wide survey of the prevalence and evolutionary forces acting on human nonsense SNPs. *Am J Hum Genet* 2009; **84**: 224–234.

305 MacArthur DG, Balasubramanian S, Frankish A *et al.* A systematic survey of loss-of-function variants in human protein-coding genes. *Science* 2012; **335**: 823–828.

306 Lim ET, Würtz P, Havulinna AS *et al.* Distribution and medical impact of loss-of-function variants in the finnish founder population. *PLoS Genet* 2014; **10**: e1004494.

307 Maurin AC, Jousse C, Averous J *et al.* The GCN2 kinase biases feeding behavior to maintain amino acid homeostasis in omnivores. *Cell Metab* 2005; **1**: 273–277.

308 Feldmann HM, Golozoubova V, Cannon B, Nedergaard J. UCP1 ablation induces obesity and abolishes diet-induced thermogenesis in mice exempt from thermal stress by living at thermoneutrality. *Cell Metab* 2009; **9**: 203–209.

309 Ward PP, Mendoza-Meneses M, Cunningham GA, Conneely OM. Iron status in mice carrying a targeted disruption of lactoferrin. *Mol Cell Biol* 2003; **23**: 178–185.

310 Ye Q, Zheng Y, Fan S *et al.* Lactoferrin deficiency promotes colitis-associated colorectal dysplasia in mice. *PloS One* 2014; **9**: e103298.

311 Safadi FF, Thornton P, Magiera H *et al.* Osteopathy and resistance to vitamin D toxicity in mice null for vitamin D binding protein. *J Clin Invest* 1999; **103**: 239–251.

312 Zella LA, Shevde NK, Hollis BW, Cooke NE, Pike JW. Vitamin D-binding protein influences total circulating levels of 1,25-

dihydroxyvitamin D3 but does not directly modulate the bioactive levels of the hormone *in vivo*. *Endocrinology* 2008; **149**: 3656–3667.

313 Booth FW, Laye MJ. Lack of adequate appreciation of physical exercise's complexities can pre-empt appropriate design and interpretation in scientific discovery. *J Physiol* 2009; **587**: 5527–5539.

314 Adams D, Baldock R, Bhattacharya S *et al.* Bloomsbury report on mouse embryo phenotyping: recommendations from the IMPC workshop on embryonic lethal screening. *Dis Model Mech* 2013; **6**: 571–579.

315 Mohun T, Adams DJ, Baldock R *et al.* Deciphering the Mechanisms of Developmental Disorders (DMDD): a new programme for phenotyping embryonic lethal mice. *Dis Model Mech* 2013; **6**: 562–566.

316 Kitsios GD, Tangri N, Castaldi PJ, Ioannidis JP. Laboratory mouse models for the human genome-wide associations. *PLoS One* 2010; **5**: e13782.

317 Georgi B, Voight BF, Bucan M. From mouse to human: evolutionary genomics analysis of human orthologs of essential genes. *PLoS Genet* 2013; **9**: e1003484.

318 Turgeon B, Meloche S. Interpreting neonatal lethal phenotypes in mouse mutants: insights into gene function and human diseases. *Physiol Rev* 2009; **89**: 1–26.

319 Grimm D. Mouse genetics. A mouse for every gene. *Science* 2006; **312**: 1862–1866.

320 Austin CP, Battey JF, Bradley A *et al.* The knockout mouse project. *Nat Genet* 2004; **36**: 921–924.

321 Donahue LR, Hrabe de Angelis M, Hagn M *et al.* Centralized mouse repositories. *Mamm Genome* 2012; **23**: 559–571.

322 Smith CM, Finger JH, Kadin JA, Richardson JE, Ringwald M. The gene expression database for mouse development (GXD): Putting developmental expression information at your fingertips. *Dev Dyn* 2014; **243**: 1176–1186.

323 Matthaei KI. Genetically manipulated mice: a powerful tool with unsuspected caveats. *J Physiol* 2007; **582**: 481–488.

324 Heffner CS, Herbert Pratt C, Babiuk RP *et al.* Supporting conditional mouse mutagenesis with a comprehensive cre characterization resource. *Nat Commun* 2012; **3**: 1218.

325 Liu Y, Strecker S, Wang L *et al.* Osterix-cre labeled progenitor cells contribute to the formation and maintenance of the bone marrow stroma. *PLoS One* 2013; **8**: e71318.

326 Chen J, Shi Y, Regan J, Karuppaiah K, Ornitz DM, Long F *et al.* Osx-Cre targets multiple cell types besides osteoblast lineage in postnatal mice. *PLoS One* 2014; **9**: e85161.

327 Brandon EP, Idzerda RL, McKnight GS. Knockouts. Targeting the mouse genome: a compendium of knockouts (Part I). *Curr Biol* 1995; **5**: 625–634.

328 Kettleborough RN, Busch-Nentwich EM, Harvey SA *et al.* A systematic genome-wide analysis of zebrafish protein-coding gene function. *Nature* 2013; **496**: 494–497.

329 The *C. elegans* Deletion Mutant Consortium. Large-scale screening for targeted knockouts in the Caenorhabditis elegans genome. *G3 (Bethesda)* 2012; **2**: 1415–1425.

330 Giaever G, Nislow C. The yeast deletion collection: a decade of functional genomics. *Genetics* 2014; **197**: 451–465.

331 Laulederkind SJ, Hayman GT, Wang SJ *et al.* The Rat Genome Database 2013—data, tools and users. *Brief Bioinform* 2013; **14**: 520–526.

Supplemental Information for this article can be found on the *Bone Research* website (http://www.nature.com/boneres).